* 56834

February 1997
Revised Edition

LAUR-95-2696

C.1

GEOLOGIC, GEOHYDROLOGIC, AND GEOCHEMICAL DATA SUMMARY OF MATERIAL DISPOSAL AREA G, TECHNICAL AREA 54 LOS ALAMOS NATIONAL LABORATORY

DONATHON KRIER, PATRICK LONGMIRE, ROBERT H. GILKESON, AND H. J. TURIN

3 9338 00688 2624

11530

Contents

1.0 INTRODUCTION ____ 1

2.0 GEOLOGY OF THE MDA G AREA ____ 2

2.1 Introduction ____ 2

2.2 Stratigraphy and Stratigraphic Nomenclature ____ 2

2.3 Description of Stratigraphic Units at Mesita del Buey ____ 4
- 2.3.1 Bandelier Tuff ____ 4
  - 2.3.1.1 Tshirege Member Unit 2b ____ 4
  - 2.3.1.2 Tshirege Member Unit 2a ____ 7
  - 2.3.1.3 Tshirege Member Unit 1b ____ 9
  - 2.3.1.4 Tshirege Member Unit 1a ____ 9
  - 2.3.1.5 Tsankawi Pumice Bed and Cerro Toledo Interval ____ 9
  - 2.3.1.6 Otowi Member ____ 10
  - 2.3.1.7 Guaje Pumice Bed ____ 10
- 2.3.2 Pre-Bandelier Tuff Units ____ 10
- 2.3.3 Alluvium and Canyon Bottoms ____ 11
- 2.3.4 Structure Sections Through the MDA G Area ____ 12

3.0 HYDROGEOLOGY OF THE MDA G AREA: FACTORS PERTAINING TO SUBSURFACE CONTAMINANT TRANSPORT ____ 12

3.1 Introduction ____ 12

3.2 Material Properties ____ 14
- 3.2.1 Density and Porosity ____ 16
- 3.2.2 Characteristic Curves ____ 16
  - 3.2.2.1 Tuff ____ 28
  - 3.2.2.2 Alluvium ____ 28
  - 3.2.2.3 Pre-Bandelier Units ____ 28
- 3.2.3 Saturated Conductivity and Unsaturated Conductivity Curves ____ 28
  - Table 3 ____ 29
  - 3.2.3.1 Tuff ____ 31
    - 3.2.3.1.1 Intact Tuff ____ 31
    - 3.2.3.1.2 Crushed Tuff ____ 32
  - 3.2.3.2 Alluvium ____ 33
  - 3.2.3.3 Pre-Bandelier Tuff Units ____ 33
- 3.2.4 Hysteresis ____ 34
- 3.2.5 Geohydrologic Properties of Rock Units beneath MDA G ____ 34

3.3 Hydrologic Conditions Below MDA G ____ 34
- 3.3.1 In Situ Moisture Content ____ 34
- 3.3.2 Perched Aquifers ____ 35
- 3.3.3 In Situ Matric Tension ____ 35

3.4 Areas for Further Investigation ____ 35

4.0 GEOCHEMICAL BASELINE INFORMATION AND DATA ____ 36

4.1 Introduction 36

4.2 Source-Term Inventory and Geochemistry 37

4.3. Geochemical Transport Parameters 40
4.3.1 Element-Radionuclide Adsorption Behavior 42
4.3.2 Element-Radionuclide Rock/Water Interactions 50
4.3.3 Element-Radionuclide Solubility Limits 51

4.4. Uncertainties and Further Investigations 53

ACKNOWLEDGMENTS 55

REFERENCES 57

APPENDIX A A-1

APPENDIX B B-1

APPENDIX C C-1

LIST OF FIGURES

1	Stratigraphic correlation chart for Bandelier Tuff, Pajarito Plateau	3
2	Location map for MDA G and nearby boreholes	5
3	Frequency distributions of fracture spacings (above) and fracture apertures (below) in Pit 39, Unit 2b	6
4	Map of elevations of basal surge deposit outcrop, Unit 2b, MDA G area	8
5	Location map for geologic structure sections, MDA G	13
6	Structure section A-C along a northwest-southeast transect, MDA G	14
7	Structure sections D-E and F-G along north-south transects, MDA G	15
8	Volumetric moisture vs. depth for 12 boreholes	20
9	Geochemical conceptual model for TA-54	39
B-1	Boreholes with moisture content profiles located in MDA L and in the proposed expansion area for Area G	B-2
B-2	Location map of boreholes and 54-1110, 54-1111, and G-5	B-3
B-3	Gravimetric core moisture content for borehole 54-1001 (angled 22°)	B-10
B-4	Gravimetric core moisture content for borehole 54-1002 (angled 22°)	B-10
B-5	Gravimetric core moisture content for borehole 54-1003 (vertical)	B-11
B-6	Gravimetric core moisture content for borehole 54-1004 (vertical)	B-11
B-7	Gravimetric core moisture content for borehole 54-1005 (angled 22°)	B-12
B-8	Gravimetric core moisture content for borehole 54-1006 (angled 27°)	B-12
B-9	Gravimetric core moisture content for borehole 54-1007 (vertical)	B-13
B-10	Gravimetric core moisture content for borehole 54-1008 (vertical)	B-13
B-11	Gravimetric core moisture content for borehole 54-1009 (vertical)	B-14
B-12	Gravimetric core moisture content for borehole 54-1010 (angled 45° below Pit A)	B-14
B-13	Gravimetric core moisture content for borehole 54-1011 (angled 35° below Pit A)	B-15
B-14	Gravimetric core moisture content for borehole 54-1012 (angled 35° below Pit B)	B-15
B-15	Gravimetric core moisture content for borehole 54-1013 (angled 35° below Pit C)	B-16
B-16	Gravimetric core moisture content for borehole 54-1014 (angled 35° below Pit D)	B-16
B-17	Gravimetric core moisture content for borehole 54-1110 (vertical)	B-17

LIST OF FIGURES

B-18	Gravimetric core moisture content for borehole 54-1111 (vertical)	B-17
B-19	Gravimetric core moisture content for borehole G-5 at MDA G (vertical)	B-18
B-20	Locations of drill holes in MDAs G and L, TA-54	B-26
B-21	TA-54 Material Disposal Area G neutron probe hole (54G-NPH) locations	B-28
B-22	Neutron moisture profile for background hole 54G-NPH-2	B-29
B-23	Neutron moisture profile for hole 54G-NPH-1, MDA G, during July–October 1994	B-29
C-1	Anemometry and permeability results, borehole 54-1001	C-15
C-2	Anemometry and permeability results, borehole 54-1002	C-15
C-3	Anemometry and permeability results, borehole 54-1003	C-16
C-4	Anemometry and permeability results, borehole 54-1004	C-16
C-5	Anemometry and permeability results, borehole 54-1005	C-17
C-6	Anemometry and permeability results, borehole 54-1006	C-17

LIST OF TABLES

1	Hydraulic properties data for MDA G stratigraphy from selected boreholes	17
2	Pressure head vs. moisture data from listed sources	22
3	Summary of geohydrologic properties beneath MDA G, Mesita del Buey	29
4	Saturated conductivity values for pre-Bandelier Tuff units	33
5	Summary of radionuclide half-lives and total activity in Pit 37 at MDA G, TA-54, November 1994	38
6	Analytical results of Water Canyon gallery groundwater, Los Alamos, New Mexico, and well J-13 groundwater, Yucca Mountain, Nevada	42
7	Average sorption ratio, K_D or R_D (ml/g) for volcanic rock, Yucca Mountain tuffs, oxidizing conditions, pH 7, 25°C	44
8	Sorption and desorption ratios, K_D or R_D (ml/g) for volcanic rock, Yucca Mountain tuffs	46
9	Average sorption ratio, K_D or R_D (ml/g) for cement [Ca(OH)2], oxidizing conditions, pH 12.5, 25°C	47
10	Ranges of sorption ratios per surface area of fractured rock, K_A (cm) for volcanic rock, Yucca Mountain tuffs and Bandelier Tuff	49
11	Ranges of retardation factors for fractured volcanic rock, K_A (cm) for volcanic rock, Yucca Mountain and Bandelier Tuff	50
12	Results of speciation investigations (measured and calculated) for selected elements at pH 7 with PCO_2 equal to $10^{-3.5}$ atm under oxidizing conditions at 25°C	52
13	Preliminary measured and calculated solubilities for selected elements in volcanic tuff at pH 7, 25°C	53
14	Preliminary measured and calculated solubilities for selected elements at pH 12, 25°C	54
B-1	Gravimetric moisture content for boreholes 54-1001 to 54-1009	B-4
B-2	Gravimetric moisture content for boreholes 54-1010 through 54-1014	B-8
B-3	Gravimetric core moisture content for boreholes 54-1110, 54-1111, and G-5	B-9
B-4	In situ gravimetric moisture content in boreholes located in natural terrain settings	B-20
B-5	Dry bulk density and calculated volumetric moisture content in core from Mesita del Buey	B-24
B-6	In situ volumetric moisture content for core from borehole LGM-85-06	B-25

LIST OF TABLES

B-7	Summary of neutron probe access holes, MDA G	B-27
C-1	Air permeability values determined from air vacuum tests and air injection tests	C-2
C-2	In situ soil-gas permeability data	C-4
C-3	In situ soil-gas permeability data	C-6
C-4	In situ soil-gas permeability data	C-8
C-5	In situ soil-gas permeability data	C-9
C-6	In situ soil-gas permeability data	C-11
C-7	In situ soil-gas permeability data	C-13
C-8	Effective air permeability determined from straddle packer tests (air extraction)	C-18
C-9	Intrinsic air permeability values on core samples	C-20

GEOLOGIC, GEOHYDROLOGIC, AND GEOCHEMICAL DATA SUMMARY OF MATERIAL DISPOSAL AREA G, TA-54, LOS ALAMOS NATIONAL LABORATORY

by

Donathan Krier, Patrick Longmire,
Robert Gilkeson, and H. J. Turin

1.0 INTRODUCTION

This report provides geologic, geohydrologic, and geochemical descriptions of rock units surrounding Material Disposal Area (MDA) G at Technical Area (TA) 54 on Mesita del Buey at Los Alamos National Laboratory (LANL), New Mexico. This information is used in the LANL performance assessment of MDA G. The assessment, which is required by Department of Energy Order 5820.2A, is an evaluation of the long-term performance of the low-level radioactive waste disposal facility and will provide dose estimates as a function of time for radionuclides migrating from the facility to various depths and available to different exposure pathways, including to the regional aquifer. We reviewed the literature, laboratory, and field data of physical and geochemical properties for lithologic units that compose the stratigraphic section beneath MDA G. The physical properties data for the rock units hosting MDA G vary in quality and in applicability to the numerical flow and transport modeling effort, which will model MDA G as specifically as possible. This report attempts to compile the most reliable and consistent data for use in the performance assessment modeling and analysis.

This report is composed of four sections and three appendices. Section 2.0 presents summary geologic information of the stratigraphic units that underlie Mesita del Buey and host, at great depth, the regional aquifer for the Pajarito Plateau. New observations from recent drilling activities are included. Section 3.0 is a compilation and discussion of the hydraulic properties of these rock units. The hydrologic information focuses on stratigraphic unit hydraulic properties measured in drill core from Mesita del Buey and adjacent canyons and follows the approach of Rogers (1994) and Rogers and Gallaher (1994a, 1994b, and 1995). The Rogers and Gallaher technical memorandums are valuable source documents for the present work and a resource for calculations of matric potential [$\theta(\Psi)$] and hydraulic conductivity [$\theta(K)$] as functions of volumetric moisture content and other physical properties of the rock matrix. The data presented draw from the measurements chosen by Rogers and Gallaher based on data reliability, but differences exist because additional data were included in this report. Section 4.0 is a review of relevant geochemical data required for solute-transport calculations and for input to the numerical model FEHM (finite element heat and mass transfer) (Zyvoloski et al. 1988) used for the performance assessment effort in modeling subsurface flow and contaminant transport. Appendix A is a reference source listing of publications cited in Sections 1, 2, and 3 and of related papers for which no journal references or LANL reports exist; reproductions of each publication are provided to the principal investigator for the MDA G performance assessment. Data from these publications were used as input to the MDA G

performance assessment modeling. Appendix B describes in situ moisture in drill cores from beneath MDA G and adjacent areas. Appendix C presents subsurface air-permeability measurements at various locations on Mesita del Buey.

2.0 GEOLOGY OF THE MDA G AREA

2.1 Introduction

Mesita del Buey is composed of layers of volcanic materials that vary in thickness from a few feet to many tens of feet. Deeper stratigraphic units include rocks of sedimentary origin. Section 2.3 describes each layer and includes discussions of transition zones between layers. An important feature is the occurrence of numerous fractures in the uppermost volcanic layers of the mesa. Descriptions of the adjacent canyons are included; they are useful for compiling a complete hydrogeologic picture of MDA G.

Geologic descriptions of the MDA G area are drawn from numerous sources. Rosenberg and Turin (1993) provide a recent summary of MDA G geologic, hydrologic, and seismologic observations. Numerous characterization studies have been undertaken over the years, and most are referenced in Rosenberg and Turin (1993) and in this report. Some of the more important studies on specific topics are by Baltz et al. (1963), Smith and Bailey (1966), Purtymun and Kennedy (1971), Kearl et al. (1986a, b), Heiken et al. (1990), and Rogers and Gallaher (1995). More recent or less available sources have been included in Appendix A.

2.2 Stratigraphy and Stratigraphic Nomenclature

Mesita del Buey is composed of a complex series of nonwelded to moderately welded rhyolitic ash-flow and ash-fall tuffs called the Bandelier Tuff (Smith and Bailey 1966, Smith et al. 1970, Heiken et al. 1990). The tuff was deposited during violent eruptions of volcanic ash from the Valles caldera, located about 18 km (11 mi.) west of MDA G. The Bandelier Tuff has two members: the Tshirege Member (upper) and the Otowi Member (lower), and both are present beneath Mesita del Buey.

Different stratigraphic systems for the Tshirege Member have been developed over the years because of local variations in lithologies. Broxton and Reneau (1995) present a correlation chart for the systems developed since 1963 for Pajarito Plateau and propose a general system that can be used across the plateau (Figure 1). That system can be applied at Mesita del Buey and currently is in use for Environmental Restoration (ER) Project drilling at TA-54. For simplicity and ease in tracking historical properties data, however, we have chosen to utilize Baltz et al. (1963) (Figure 1) because of its widespread use in many physical properties investigations related to MDA G and to other waste disposal and hydrologic issues at the Laboratory.

From the surface downward, stratigraphic units beneath TA-54 consist of the Tshirege Member of the Bandelier Tuff (Units 2b, 2a, 1b, and 1a, and the basal Tsankawi pumice bed) and the Otowi Member of the Bandelier Tuff with its basal Guaje pumice bed. The members are separated by an ash-fall/fluviatile sedimentary interval (Cerro Toledo interval). Underlying the tuff is a thin deposit of poorly sorted coarse sandstones alternating with ashy layers, assigned to the Puye Formation; a thick sequence of basalt

flows and breccias of the Cerros del Rio basalts; and conglomerates and sandstones of the Puye Formation, which host the regional aquifer. From the region surrounding MDA G, Units 2b through 1b crop out on the tops and sides of Mesita del Buey, and all rocks that predate Unit 1b are observed only in boreholes penetrating below the base of the mesa. At Mesita del Buey, the potentiometric surface of the regional aquifer is at an elevation of about 1768 m (5800 ft) (Purtymun 1984). The mesa top elevation at MDA G is approximately 2048 m (6720 ft).

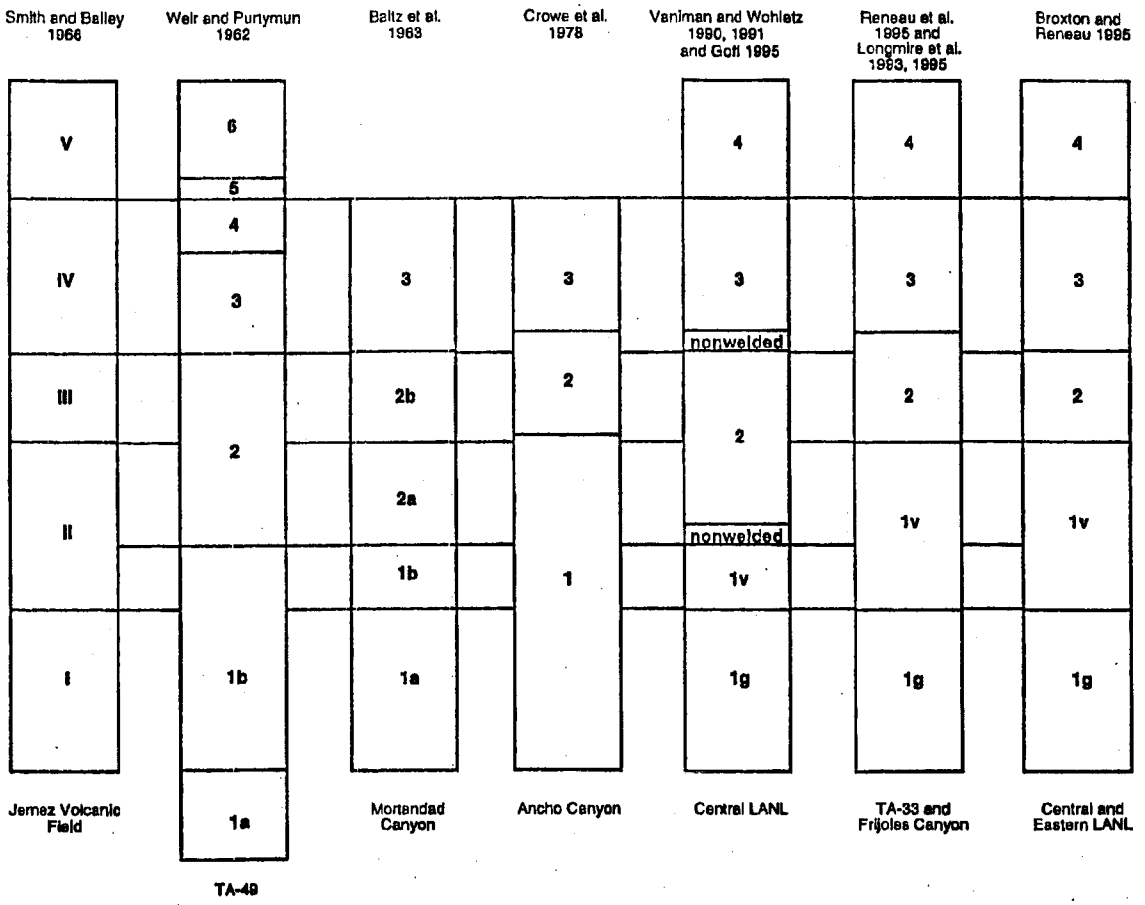

Figure 1. Stratigraphic correlation chart for Bandelier Tuff, Pajarito Plateau (Broxton and Reneau 1995).

The scope of available data specific to MDA G is limited. Hydraulic data do not exist for units deeper than the Otowi Member. Data on fractures are limited to Units 1b, 2a and 2b, which crop out on the top and sides of the mesa, and these data are incomplete because of limited exposure. A few boreholes in the area adjacent to MDA L extend to depths of about 100 m (328 ft), but within MDA G no boreholes extend deeper than about 45 m (148 ft).

2.3 Description of Stratigraphic Units at Mesita del Buey

The following sections contain descriptions of the stratigraphic units at Mesita del Buey. These units have wide distribution across the Pajarito Plateau except for the deeper basaltic lava flows section. The basaltic lava flows are limited to the eastern and southeastern plateau. Some descriptions are drawn from recent lithologic logging in boreholes near MDA L by F. Caporuscio (1994) and J. Marin (LANL, in progress). Broxton et al. (in progress) give detailed petrographic and geochemical descriptions of the units beneath the mesa. Figure 2 gives location information for MDA G and nearby boreholes.

2.3.1 Bandelier Tuff

2.3.1.1 Tshirege Member Unit 2b

Unit 2b is a brittle resistant caprock that forms the top of Mesita del Buey and adjacent mesas. It is the distal part of an extensive ash-flow sheet that is moderately welded and about 12 m (39 ft) thick at MDA G. This uppermost stratigraphic unit hosts the disposal pits and shafts that are the focus of the performance assessment.

Unit 2b is composed of crystal-rich devitrified pumice fragments in a matrix of ash, shards, and abundant phenocrysts. The rock is extensively fractured because of the contraction of the welded ash matrix as it cooled after deposition. The vertical cooling fractures have been described in several studies, but most thoroughly in studies of Disposal Pit 39 (Reneau and Vaniman 1994) and of the north wall of Pajarito Canyon (Reneau et al. 1995).

Maps of Pit 39 show that the mean fracture spacing in Unit 2b ranges between 0.6 and 0.8 m (1.9 and 2.6 ft), and apertures range between <1 and 13 mm (<0.03 and 0.51 in.) with a median of 3 mm (0.1 in.) (Figure 3). Previous fracture mapping in disposal pits (Purtymun and Kennedy 1971, Purtymun et al. 1978) indicated larger spacing (about 2.2 m, 7.1 ft); this may be attributable to incomplete mapping of minor fractures on the pit walls. Fracture orientations vary in Pit 39, but greatest frequencies are in the N 50° E and east-west directions. Fracture dip in Unit 2b averages 90° (vertical).

In Pit 39, fractures are typically filled with smectite clays to a depth of 3 to 4 m (9.8 to 13.1 ft) and with opal and calcite below this depth. Opal and calcite deposition is associated with presence of tree root molds. The association suggests that biological activity or its cessation results in mineral precipitation, which works to partially occlude transport pathways. In a root study, Martens and Barnes (1993) found the distal ends of roots of living piñon trees in thin joints at depths of 14 m (46 ft) in Pit 39, a fact often cited as evidence of moisture availability to this depth in the tuff. Living roots were observed to the bottom of the pit at a depth of 14.2 m (45 ft) (Reneau and Vaniman); their maximum depth is unknown. Observations in neighboring Pit 38 reveal one set of live roots at a depth of about 20 m (66 ft). The 3- to 4-mm-diameter (~0.1 in.) roots have grown downward within a prominent, near vertical fracture that is filled with clay and extends from the surface to below the bottom of the pit.

Deposition by wind and/or water of clays and carbonates in fractures is demonstrated by Davenport (1993) in a study at MDA J, about 2 km (1.2 mi.) northwest of MDA G. In

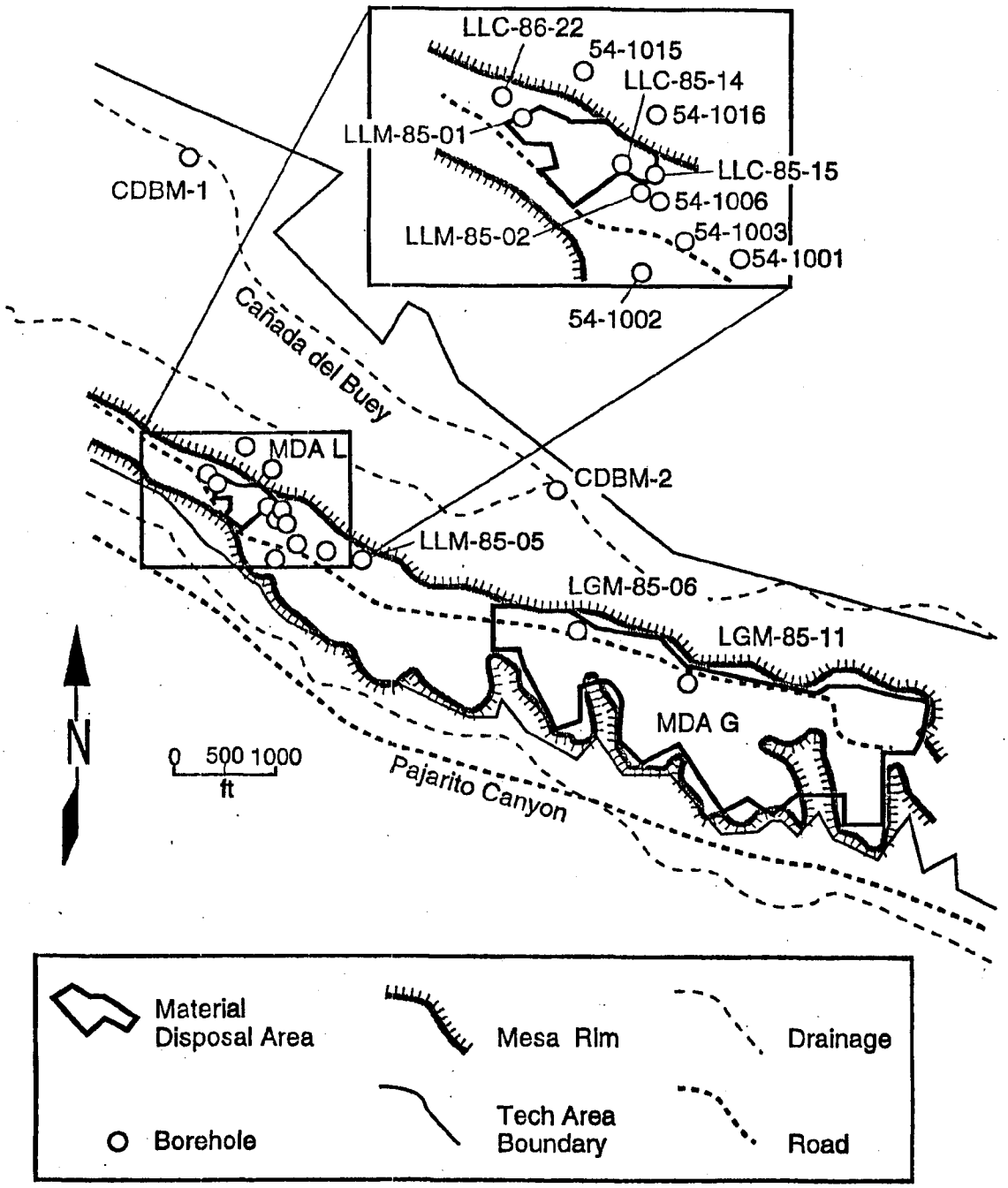

(Rogers and Gallaher 1994b)

Figure 2. Location map for MDA G and nearby boreholes.

detail, calcium carbonate deposition is usually interior to clay deposition where they coexist within a fracture. In Davenport's model, calcium carbonate precipitates from percolating water trapped in smectite shrinkage cracks as the clays rehydrate and swell. The swelling lowers fracture permeability within the upper several meters of fractured tuff. He concludes that the presence of calcite within clay fillings suggests that "clay fill alone does not completely seal the fractures or preclude water movement through them."

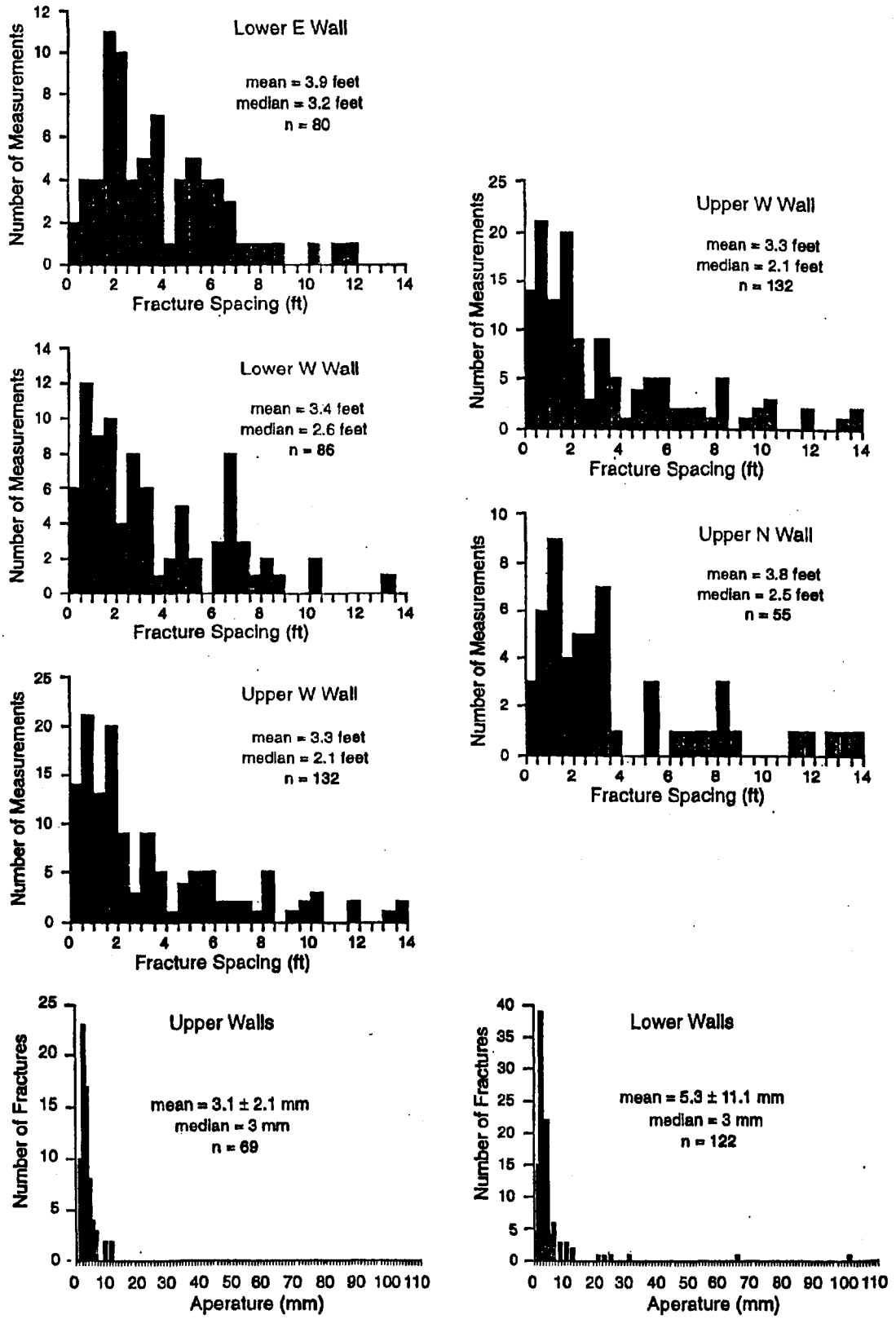

Figure 3. Frequency distributions of fracture spacings (above) and fracture aperatures (below) in Pit 39, Unit 2b (Reneau and Vaniman 1994).

Kearl et al. (1986a, b) report an increase in the number of fractures within more welded portions of Units 2b and in underlying Units 2a and 1b. A much smaller population of fractures is observed in the nonwelded to slightly welded Unit 1a. They describe one case of a dense lining (*case hardening*) along a cored fracture in Unit 2b at a depth of 10.0 to 13.4 m (35 to 44 ft), which they suggest may indicate preferential flow of water or water vapor in the fracture at that depth. Furthermore, their gravimetric moisture content data show increases in moisture associated with two specific fractures at depths of 11.6 m and 13.8 m (38 and 55 ft).

Recent ER Project drilling at the TA-73 landfill (airport site) has revealed elevated moisture associated with fractures at depths to 41 m (135 ft). Detailed fracture mapping along outcrops at TA-73 has demonstrated intervals of increased fracture density for tuff in cliff exposures. The development of these intervals is attributed to the strain response of brittle, moderately welded tuff to tectonic movement in the deeper subsurface rather than to cooling contraction immediately after deposition (Matt Walters, personal communication, 1995). Differential block motion along cooling fractures or planes of weakness is also evident. Along Mesita del Buey, this type of detailed fracture mapping has not been done.

A thin (<10 cm, <4 in.) interval of crystal-rich, fine sand-sized material is commonly found at the base of Unit 2b. This interval of lenticular and sometimes cross-bedded layers is attributed to deposition from the basal surge associated with violent eruptions. It rises in stratigraphic position 1 to 3 m (3 to 10 ft) toward the west (Broxton et al., in progress). In eastern TA-54, these layers (surge beds) occupy the highest levels of Unit 2a and progressively climb in stratigraphic position westward beyond MDA G where they occupy the basal portion of Unit 2b. The elevations of the surge beds have been surveyed on the edges of Mesita del Buey and are shown in Figure 4 (D. Broxton, personal communication, June 1995). The surge beds are displaced by small faults; displacements range between 5 cm (2 in.) and 60 cm (23.6 in.), with relative motions down to the west. Twenty-six such faults were measured along the north wall of Pajarito Canyon, but the number may be greater because of poor exposure in some areas. These small faults appear along cooling joints in the upper part of Unit 2b, but they have no aperture at the elevation of the surge beds. It is not known whether the faults die out in underlying poorly welded tuffs, as the majority of cooling joints do. There is evidence from borehole packer tests (Appendix C) that the thin surge beds allow higher air flow within the mesa interior because of impinging winds and fluctuations in barometric pressure.

2.3.1.2 Tshirege Member Unit 2a

Tshirege Member Unit 2a underlies Unit 2b and consists of devitrified ash-fall and ash-flow tuff (Purtymun and Kennedy 1971, Kearl et al. 1986a, b). The unit is about 14 m (46 ft) thick near MDA G, is slightly welded at its base, and becomes moderately welded up section. In outcrop, it has a massive and unjointed appearance, but its upper parts host downward extensions of more prominent cooling fractures that originate in Unit 2b. In outcrop and limited angled borehole data, the fractures die out downward as the tuff becomes less consolidated. Because of the very weak nature of the unit, attempts at retrieving core from Unit 2a near MDA L during ER Project investigations (Fall 1993, Summer 1994) invariably resulted in unconsolidated material.

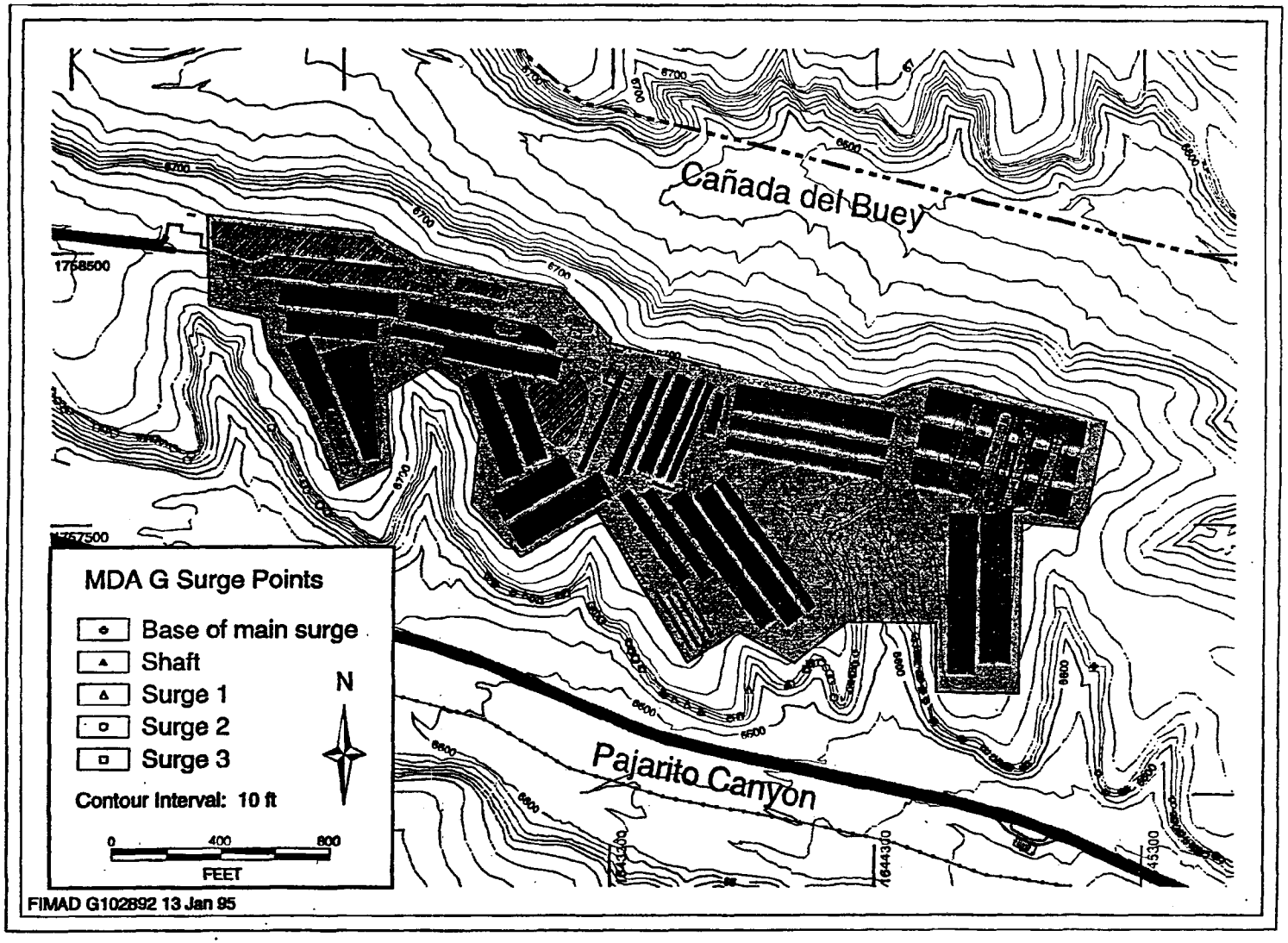

Figure 4. Map of elevations of basal surge deposit outcrop, Unit 2b, MDA G area.

2.3.1.3 Tshirege Member Unit 1b

Kearl et al. (1986a, b) describe Unit 1b as a slightly welded, devitrified ash-flow tuff at its base and top that becomes more welded in its center. However, the unit never exhibits the jointing characteristics of moderate welding shown by Unit 2b, which caps the mesa. Unit 1b is 7 to 8 m (23 to 26 ft) thick in eastern MDA G and 15 m (49 ft) thick near MDA L. It has a greater content of unflattened (nonwelded) pumice lapilli (size of 4 to 32 mm, 0.1 to 1.3 in.) than the overlying tuff (Unit 2a), which may contribute to a decreased density (Kearl et al. 1986a, b). The pumices are devitrified and show spherulitic cristobalite structures but become slightly more vitric with depth.

Unit 1b is more resistant to erosion that overlying Unit 2a and can form a small ledge in weathered outcrops. In the outcrop, the tuff hosts closely spaced (7.6 to 12.7 cm, 3 to 5 in.) vertical fractures that give the tuff an appearance of vertical colonnades.

Unit 1b is exposed at the base of the south-facing slope of Mesita del Buey. In drill core, its basal contact is marked by a rapid change [vertical distance of ~0.2 m (~0.7 ft)] from devitrified to vitric glass in underlying Unit 1a. Vitric pumices below this interval stand out in relief on weathered surfaces; devitrified pumices above this interval are eroded out leaving holes that wind, water, and ice continue to enlarge. This transition results in a preferentially eroded recess defined by alignment of small caves, some as tall as 1.5 m (5 ft); this recess is named the vapor-phase notch by Baltz et al. (1963). Characteristics of this interval at TA-21 are summarized by Broxton et al. (1995).

2.3.1.4 Tshirege Member Unit 1a

Unit 1a is the oldest unit of the Tshirege Member. It is a vitric, pumiceous, nonwelded ash-flow tuff that has a thickness of about 15 m (49 ft) beneath MDA G. Purtymun (1995) observed thicknesses in drill holes ranging between 15 m (49 ft) east of MDA G and 13 m (43 ft) west of MDA G. Further west, drilling beneath MDA L has penetrated 36 m (118 ft) of Unit 1a. Outcrops on south-facing slopes near MDA G suggest 15 m (49 ft) as a minimum thickness, perhaps because of local thickening from north to south through the mesa. There is little information about extent or characteristics of fractures in this unit. Kearl et al. (1986a, b) report encountering only 2 fractures in 11 holes cored into Unit 1a, although the entire thickness of the unit was never penetrated. Typically, nonwelded tuffs do not support fractures because of their weak matrix properties and relatively cool temperature at deposition.

2.3.1.5 Tsankawi Pumice Bed and Cerro Toledo Interval

The Tsankawi pumice bed near MDA G is a thin (<0.3 m, <1.0 ft) layer of gravel-sized, vitric, nonwelded pumice. Its presence is widespread across the Pajarito Plateau at the base of the Tshirege Member. The Cerro Toledo interval stratigraphically underlies the Tsankawi pumice bed and is composed of interbedded and lenticular beds of tuffaceous sandstones, siltstones, ash and pumice falls, and intercalated gravel and cobble deposits derived from mafic to intermediate lavas of the Tshicoma Formation. Some layers show evidence of reworking by running water during or soon after deposition.

The distinct Tsankawi pumice bed and the Cerro Toledo interval separate the upper and lower tuff members of the Bandelier Tuff but were often included as part of the top of the

underlying Otowi Member tuffs during past core logging at TA-54. In recent drilling beneath MDA L, 9 m (29 ft) of Cerro Toledo interval and <0.5 m (1.6 ft) of overlying Tsankawi pumice bed were encountered. Because the Cerro Toledo interval thins eastward across the Pajarito Plateau, we assign a 5-m (16-ft) thickness to this interval beneath MDA G. Physical properties of this interval would probably be dominated by Cerro Toledo sedimentary beds because the Tsankawi pumice bed is very thin. In borehole 54-1015 (Figure 2), Cerro Toledo interval core was damp with moisture and was the shallowest visible moisture encountered in the borehole (elevation 1994.3 m, 6543 ft). No contaminants have been measured with field instruments or in core sample analysis in this interval.

2.3.1.6 Otowi Member

Otowi Member tuffs are about 30 m (98 ft) thick beneath MDA L and thin eastward toward MDA G. No complete thickness has been measured for MDA G. The tuffs are composed of a massive, nonwelded, pumice-rich, mostly vitric ash-flow tuff. Pumices are fully inflated, meaning that the tubular pumice structures are not collapsed by any postdepositional welding. Beneath MDA L, the pumice makes up about 20% of the tuff, ranges in size between 0.5 and 7.0 cm (0.2 and 2.8 in.), and is vitric. The matrix is an unsorted mix of glass shards, phenocrysts, perlite clasts, and minute broken pumice fragments. Lithic fragments make up about 2% of the rock, and rare pumice swarms (with up to 30% pumice) occupy intervals as much as 0.6 m (2 ft) thick. No visible moisture has been observed in cored Otowi Member beneath Mesita del Buey.

2.3.1.7 Guaje Pumice Bed

The Otowi Member overlies 3 m (10 ft) of the Guaje pumice bed at a depth of 117.6 m (386 ft) beneath MDA L, corresponding to an elevation of 1955 m (6414 ft). The unit is composed entirely of pumices ranging between 0.3 and 1.5 cm (0.1 and 0.6 in.) in diameter. The pumice fragments are nonwelded but silicified and brittle beneath MDA L. Pumice tubes are partially filled with silica cement and may have reduced matrix permeability near that locality. The Guaje pumice bed is reported as 3.7 m (12 ft) thick in well T-5, located in Pajarito Canyon south of MDA G. Correlations between boreholes at MDA G suggest a shallow southward component of dip to the Guaje pumice bed.

2.3.2 Pre-Bandelier Tuff Units

In borehole 54-1015 at MDA L, the base of the Guaje pumice bed overlies about 3 m (10 ft) of poorly consolidated, interbedded, coarse sand, silt, and ashy layers that are probably related to the Puye(?) Formation. The thin finer-grained layers in the core were damp, but the basalt immediately below the contact was dry.

Layers of thick mafic lava flows and flow breccias of the Cerros del Rio basalts underlie the thin interval of Puye Formation. Little is known about fractures and internal contacts within the Cerros del Rio basalts beneath MDA G. Exposed basaltic flows in steep canyons on the Pajarito Plateau are highly fractured; discontinuous fractures form a jagged network with unfilled open apertures. Flow breccias are found separating individual flows and occupying the toes of flow fronts. Breccias are more easily eroded in outcrop and do not support fractures extending through the denser lava flows.

The Cerros del Rio basalts have been cored in boreholes 54-1015 and 54-1016 in the canyon north of MDA L. They consist of rubbly flow breccias and dense fractured microporphyritic lava flows with up to 10% vesicles, with zones of moderately vesicular to very frothy lavas (as much as 60% open vesicles) in the uppermost 21 m (69 ft). In borehole 54-1015, the circulation of drill air and retrieval of cuttings were lost when the drill encountered the frothy basaltic lava from about 100 to 105 m (328 to 345 ft); this indicated high permeability of the frothy basalts. On the other hand, drill air and cuttings were returned in the denser basaltic lavas, and little loss of circulation occurred through these intervals. However, during drilling of borehole 54-1016 at a depth of 33 m (108 ft) below the top of the basalt, the drill air was observed blowing out from borehole 54-1015, 107 m (351 ft) east of 54-1015. Both holes were uncased within the basalt. An ~500 ft^3/min. blower had been used for drilling borehole 54-1016, but the borehole had completely lost circulation, and an estimated 5 to 10% of the injection air had flowed to the distant well (J. Eddy, personal communication, March 1995). The observed flow of drill air horizontally through the basalt indicates high permeability in the frothy basaltic section.

Total thickness of the Cerros del Rio basalts beneath MDA G is unknown. In borehole 54-1015, a thickness of 48 m (157 ft) of basalts were drilled with no lower contact encountered. Puye Formation sedimentary rocks were encountered beneath 82 m (269 ft) of basalt in well PM-2, located south of MDA L. No basal contact was encountered in well T-5, south of MDA G, after drilling through 28 m (92 ft) of basalt.

Elevation of the top of the basalt directly beneath MDA L in borehole 54-1015 is 1949.5 m (6396 ft) above sea level. Hole LGC-89-32 in western MDA G encountered basalt at 1967.2 m (6454 ft) elevation; hole LGC-89-33 in eastern MDA G encountered basalt at 1980.7 m (6498 ft) elevation; and well T-6, south of MDA L, encountered basalt at 8133 m (6015 ft) elevation (Purtymun 1995). These elevations indicate that the basalt dips about 5° toward the west and possibly steepens east of MDA G toward basalt outcrops at State Road 4 and Pajarito Road. Basalt rock textures similar to those found near surface volcanic vents have been located near this intersection, about 1 km (0.6 mi.) east of MDA G.

Underlying and interfingering with the basalts are sedimentary conglomerates and fanglomerates of the main body of the Puye Formation. The upper approximately 200 m (656 ft) are composed of coarse basaltic, latitic, and quartzite gravels in a poorly sorted matrix of sand- and silt-sized grains. Well PM-2, located about 1.5 km (0.93 mi.) west of MDA G, is the nearest hole to intercept the Puye Formation and underlying Tesuque Formation, which host the regional aquifer (Cooper et al. 1965, Purtymun and Cooper 1969). No boreholes at MDA G extend deep enough to encounter these deeper units.

2.3.3 Alluvium and Canyon Bottoms

The canyons that bound Mesita del Buey in the region of MDA G are Pajarito Canyon to the south and Cañada del Buey to the north (Figure 2). Canyon alluvium is composed of unconsolidated silty to coarse sands of quartz and sanidine feldspar crystals, crystal fragments, and broken pumice fragments weathered from the surrounding mesa tops and sides. Occasionally, fragments of latite or similar composition lava are incorporated, as are cobble- or smaller-size fragments of welded tuff. Alluvial packages are lensoid in cross section and reach 3 to 4 m (10 to 13 ft) in thickness (Purtymun 1995).

The canyons transport water and loose sediment by way of surface runoff from the mesa and flow originating upstream from MDA G. Pajarito Canyon, on the south side of Mesita del Buey, transmits water intermittently throughout seasons of heavy precipitation. Cañada del Buey, on the north side, drains a much smaller area and flows only during heavy snowmelt or heavy rains. Pajarito Canyon hosts a known narrow alluvial aquifer system in an area near but upstream of MDA G. However, drilling within Cañada del Buey near MDA G shows that these canyon sediments contain no perched water, although thin moist lenses of silt and clay are reported (Devaurs 1985, Devaurs and Purtymun 1985, Purtymun 1995). (Perched water, probably related to discharge from a nearby water supply well, is reported in two boreholes in Cañada del Buey approximately 1800 m (6000 ft) upstream from MDA G; see Purtymun 1995, p. 114.).

2.3.4 Structure Sections Through the MDA G Area

Figure 5 indicates the lines of structure sections shown in Figures 6 and 7. Geologic controls for the sections are from boreholes shown on the figures. Bandelier Tuff units thin from west to east and dip about 3° to the east; borehole data suggest very little southeast component of dip to these sheet-like deposits, but measurements on outcrops at MDA G indicate a strike and dip on Unit 2b of approximately N 68° E 3° SE. The Bandelier Tuff is about 90 m (295 ft) thick beneath the west boundary of MDA G and 44 m (144 ft) thick beneath the east boundary. The thickness of Unit 2a in hole LGM 85-11 suggests a southerly component of dip to its upper contact, but other unit thicknesses are consistent with a gentle eastward dip. The Guaje pumice bed has been identified in the western map area, but the unit, if present, is very thin in the east.

Other than the minor faults described above at the base of Unit 2b of the Tshirege Member, no geologic faults or surface expressions of buried structure have been identified at Mesita del Buey. Cooling joints in the tuffs provide the only known fracture flow paths within the Bandelier Tuff.

3.0 HYDROGEOLOGY OF THE MDA G AREA: FACTORS PERTAINING TO SUBSURFACE CONTAMINANT TRANSPORT

3.1 Introduction

The portion of the performance assessment to which this document pertains is concerned with radionuclide contaminant transport beneath MDA G. If such subsurface transport is significant, it will be controlled by flow processes. The processes that drive flow and transport at MDA G are extremely complex, involving two phases (liquid and gas) in a variably saturated medium. The system is further complicated by the presence of open to filled fractures. Liquid flow in the partially-saturated (vadose) zone above the water table is driven by energy gradients and controlled by the hydraulic conductivity and structure of the medium. At the same time, the gradients and the conductivity are strongly affected by the moisture content distribution. This interrelated feedback system results in complex nonlinear behavior that is described by nonlinear partial differential equations. These equations cannot be solved analytically, so to accurately predict fluid movement and distributions, it is almost always necessary to use a numerical modeling approach. The accuracy of the numerical model depends on the accuracy of the characterization of the system. This includes knowing the values of the different material properties and

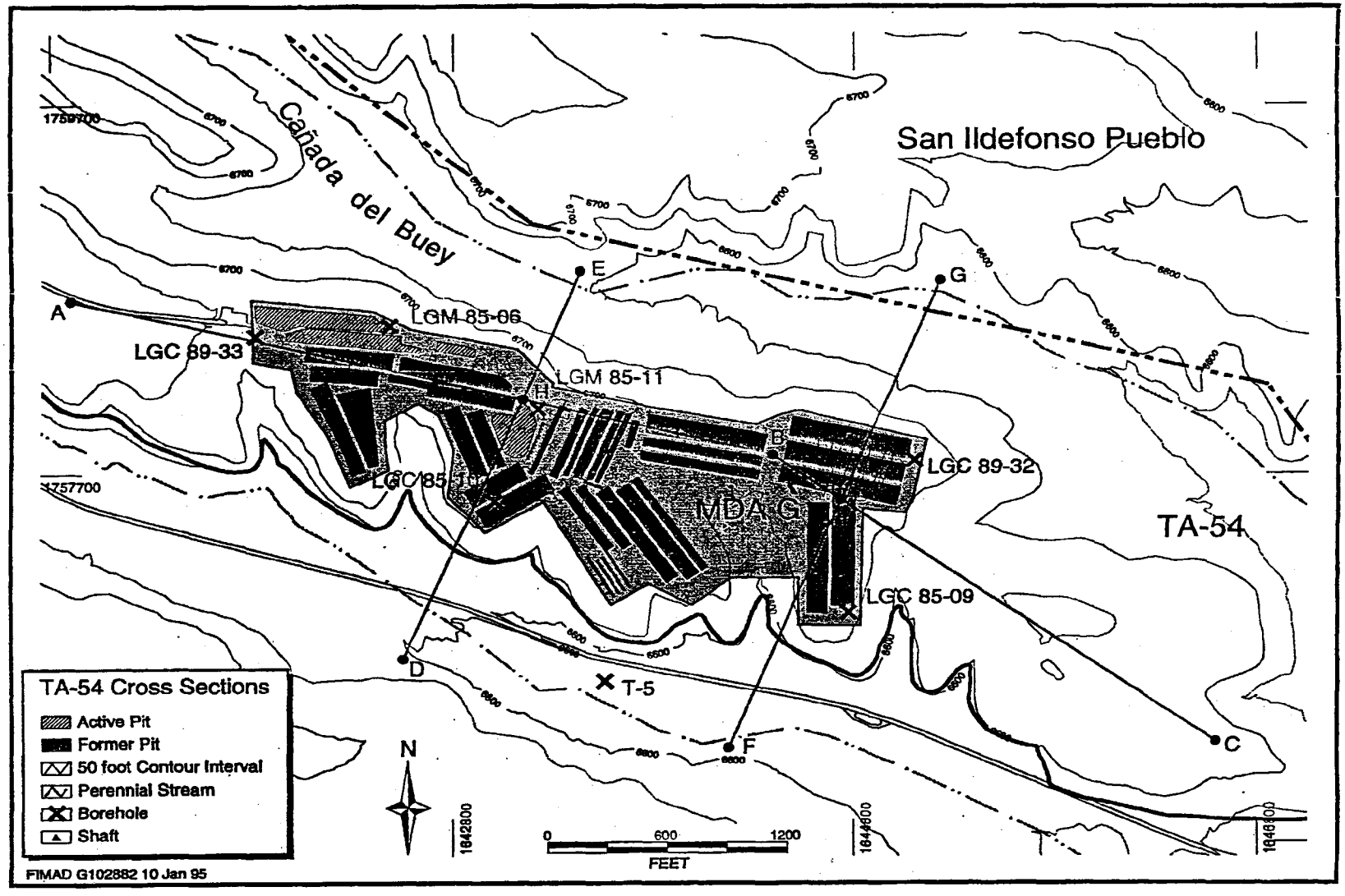

Figure 5. Location map for geologic structure sections, MDA G.

relationships called for in the equations. The purpose of this section is to summarize available data on material properties, report values that are representative of the different hydrogeologic units under MDA G, and provide references to the original data sources.

Most of the data presented or referenced in this section pertain to the upper Bandelier Tuff units because those are the units in which virtually all of the cores and measurements have been taken. The approximately 190 m (623 ft) of basaltic and underlying sedimentary rocks between the Bandelier Tuff and the water table have never been cored beneath MDA G and have rarely been cored elsewhere on the Pajarito Plateau, and thus, the hydraulic properties are largely unknown. Once measured, they would provide additional information on radionuclide transport times away from the disposal areas.

3.2 Material Properties

Some material properties and relationships are needed to characterize the subsurface system. Rock properties include porosity, bulk density, and saturated hydraulic conductivity. Properties that characterize the fluid/rock relationships in the vadose zone include θ, the volumetric moisture content (a measure of the amount of water present); ψ, the matric potential (suction, tension) (a measure of the energy state of the water); and K, the hydraulic conductivity (a measure of the ability of a fluid to flow). These three properties are strongly interrelated. The relationships between them are called *constitutive relationships* and include the θ-ψ relationship, the *characteristic curve*, and the K-θ and K-ψ relationships, the *unsaturated conductivity curves*. In the following tables, we have compiled values for these properties and relationships.

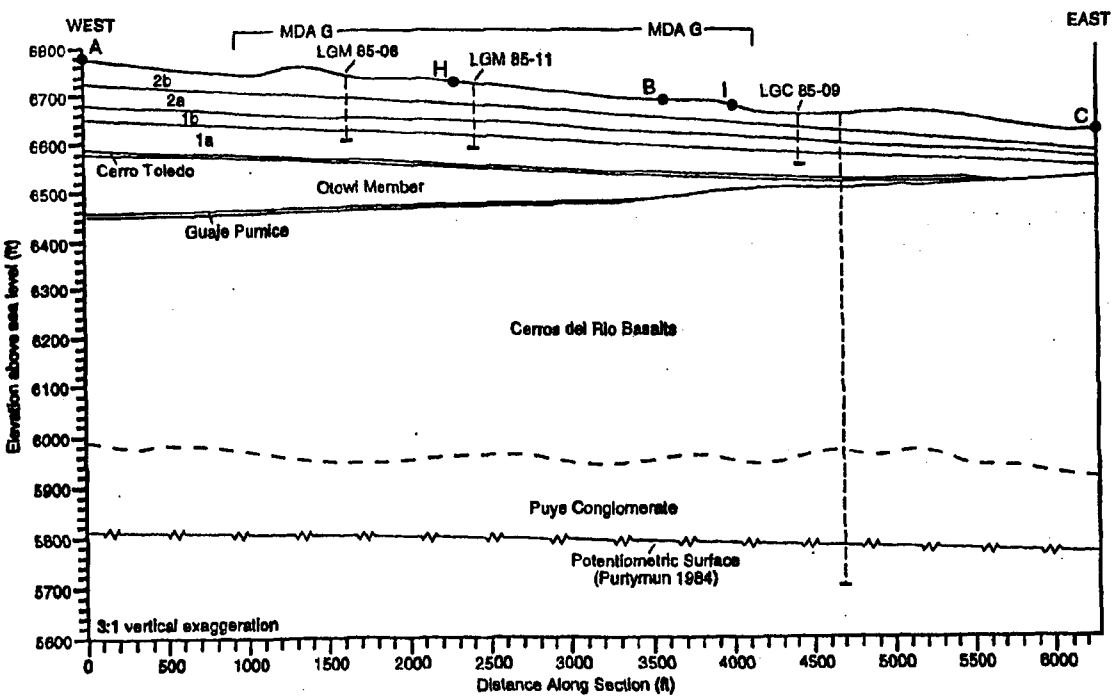

Figure 6. Structure section A-C along a northwest-southeast transect, MDA G.

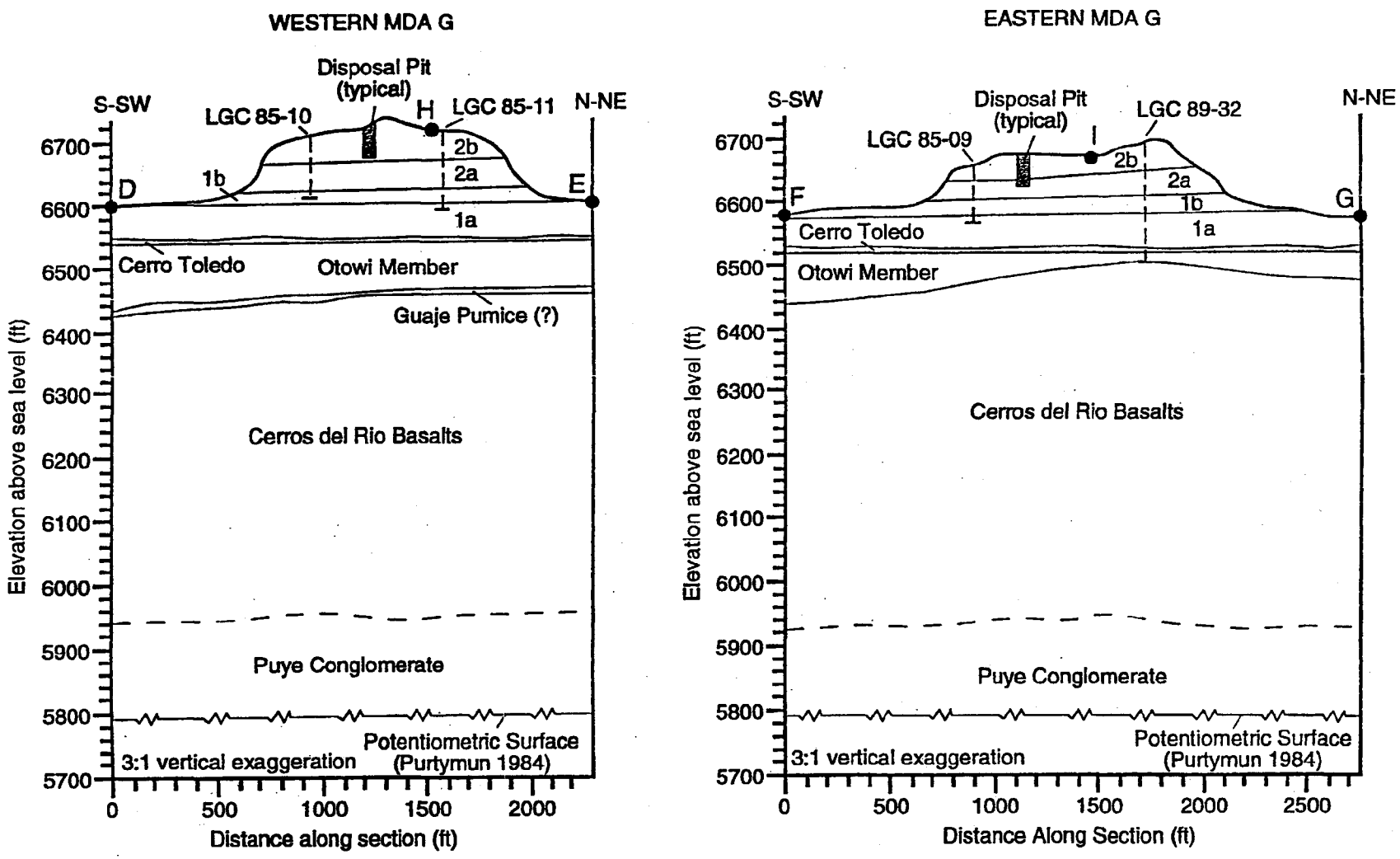

Figure 7. Structure sections D-E and F-G along north-south transects, MDA G.

Table 1 lists published and unpublished hydraulic property data measured from selected cores of MDA G and the vicinity. The data listed represent the best available based on the stratigraphic assignments of the samples, the analytical procedure used, and traceability of the data. However, in the case of stratigraphic assignments in Kearl et al. (1986a, b), we have reassigned a thickness of 8 m (26 ft) to Unit 1b, based on measured thicknesses in several outcrops and comparisons between the section originally described at Mortandad Canyon (Baltz et al. 1963) and Mesita del Buey. In doing so, we moved core measurements from upper Unit 1b (Kearl et al. 1986a, b) to their correct assignment in lower Unit 2a. This reassignment affects only three samples.

Individual sample data in Table 1 come from a variety of sources. For 16 of the samples in Table 1, volumetric water content was estimated from core moisture profiles reported in Kearl et al. (1986a, b). The original plots of the core moisture data as a function of depth are reproduced in Figure 8. The estimated data are sufficiently similar among the holes and agree sufficiently well with recently measured values that this approximation is acceptable for characterization of these layers.

3.2.1 Density and Porosity

Porosity is used in equations for flow and transport. Both porosity and bulk density are needed when converting moisture content to saturation, which is the form used in the model calculations. Numerous density and porosity measurements on Bandelier Tuff in the vicinity of MDA G have been reported by Kearl et al. (1986a, b) and in various reports by Stephens and Associates, Inc. (1994a, 1992b, 1992a, 1991), as summarized by Rogers and Gallaher (1994b).

In general, the best published descriptions of the pre-Bandelier units in the vicinity of MDA G are the drilling logs from water supply wells PM-1 and PM-2, (Cooper et al. 1965). However, no density or porosity measurements are reported.

3.2.2 Characteristic Curves

The characteristic curve (θ vs. ψ) is needed for any numerical prediction of flow in the unsaturated zone and can also be used for estimating field head (ψ) gradients from more readily available θ measurements. The determination of the characteristic curve for a core sample can be found in Bear (1972) and Klute (1986) and provides the types of data listed in Table 2.

Table 2 lists the moisture characteristics of drainage curves (water displaced by air), as measured in laboratory experiments on 45 samples of tuff. Data sources are shown after the table. The values reported in Table 2 use pressure-plate-derived data up to pressures of about 1 bar (-1021 cm) and psychrometer-derived data at the higher values of tension. Rogers and Gallaher (1994b) discuss the rationale for accepting measurements in reports from the geotechnical laboratory of Daniel B. Stephens and Associates and from Bendix (Kearl et al. 1986a, b). Because pressure-plate measurements do not equilibrate above ~0.5 bar (-511 cm water), psychrometer measurements should be used in high-tension regimes (Stephens and Associates 1992a).

TABLE 1

HYDRAULIC PROPERTIES DATA FOR MDA G STRATIGRAPHY FROM SELECTED BOREHOLES

Tshirege Member, Unit 2b

Borehole	Depth (ft)	ρ_b (g/cm^3)	θ (vol. %)	Porosity (%)	Saturation (%)	K_{SAT} (cm/sec)	θ_r (%)	N	α
LGM 85-11	3	—	—	54.0	—	5.4×10^{-4}	—	—	—
LLM 85-02	7	—	—	41.5	—	4.4×10^{-4}	—	—	—
5 LLC 85-15	10.0	1.46	1.0	46.4	2.2	1.6×10^{-3}	3.8	2.044	.0060
LLM 85-05	15	—	0.7*	52.6	1.3	5.4×10^{-4}	—	—	—
LGM 85-06	29	—	1.0*	42.5	2.4	4.8×10^{-4}	—	—	—
8 LLC 85-14	29.0	1.39	2.0	44.1	4.5	4.2×10^{-4}	0.0	1.890	.0060
LGM 85-11	30	—	1.9*	51.5	3.7	2.8×10^{-4}	—	—	—
LLM 85-01	30	—	3.8*	39.6	9.6	1.1×10^{-4}	—	—	—
LLM 85-02	36	—	3.7*	46.5	8.0	1.2×10^{-4}	—	—	—
LLM 85-05	36	—	2.0*	73.6	2.7	2.2×10^{-4}	—	—	—
54-1006	41.5	1.28	4.7	44.9	10.5	4.1×10^{-4}	0.0	1.760	.0064
LGM 85-06	51	—	1.3*	40.2	3.2	8.4×10^{-5}	—	—	—

Tshirege Member, Unit 2a

Borehole	Depth (ft)	ρ_b (g/cm^3)	θ (vol. %)	Porosity (%)	Saturation (%)	K_{SAT} (cm/sec)	θ_r (%)	N	α
LLM 85-01	52	—	1.3*	64.4	2.0	2.7×10^{-4}	—	—	—
2A LLC 86-22	54.5	1.26	1.3*	51.0	2.5	8.2×10^{-5}	2.0	2.238	.0037
2B LLC 86-22	54.5	1.26	1.3	48.3	2.7	2.5×10^{-4}	0.0	1.932	.0045
7 LLC 86-22	65.0	1.27	1.4*	48.7	2.9	1.4×10^{-4}	0.0	2.347	.0026
LLM 85-02	67	—	1.3*	43.3	3.0	9.8×10^{-5}	—	—	—
54-1001	67.8	1.20	1.9	41.4	4.6	1.3×10^{-4}	0.0	1.894	.0034
LLM 85-05	76	—	2.6	74.2	3.5	1.3×10^{-4}	—	—	—
54-1006	76.2	1.28	0.6	44.5	1.3	9.8×10^{-5}	0.0	1.880	.0030
54-1001	82.5	1.25	2.6	46.0	5.7	1.1×10^{-4}	0.0	2.225	.0022
54-1002	91.8	1.26	1.5	46.0	3.3	8.1×10^{-5}	0.0	2.213	.0012
LLM 85-01	101	—	3.4*	62.1	5.5	2.5×10^{-4}	—	—	—
54-1001	101.5	1.19	3.9	51.4	7.6	1.6×10^{-4}	0.0	1.782	.0034
54-1003	101.5	1.22	1.5	51.0	2.9	1.3×10^{-4}	0.0	1.733	.0030

* Moisture content (θ) estimated from moisture profiles in Kearl et al. (1986a, b).

TABLE 1 (continued)

Tshirege Member, Unit 1b									
Borehole	Depth (ft)	ρ_b (g/cm^3)	θ (vol. %)	Porosity (%)	Saturation (%)	K_{SAT} (cm/sec)	θ_r (%)	N	α
LGM 85-11	94	—	14.6*	64.3	22.7	1.1×10^{-4}	—	—	—
LLM-85-06	99	—	11.0*	52.6	20.9	1.3×10^{-3}	—	—	—
LLM 85-02	117	—	8.4*	48.5	17.3	1.7×10^{-4}	—	—	—
54-1003	119.0	1.22	6.4	59.9	10.7	9.9×10^{-5}	—	—	—
54-1001	121.5	1.18	9.0	46.4	19.4	2.2×10^{-5}	0.0	1.583	.0041
54-1002	121.5	1.23	3.2	49.5	6.5	4.6×10^{-5}	0.0	1.773	.0031
54-1006	124.0	1.22	2.5	43.5	5.7	4.5×10^{-5}	0.0	1.721	.0035
1 LLC 86-22	131.5	1.05	20.0*	50.7	39.4	1.9×10^{-5}	1.2	1.586	.0021
1BLLC 86-22	131.5	1.05	22.0	50.8	43.3	2.7×10^{-5}	4.4	1.709	.0021
54-1006	136.0	1.28	6.3	47.2	13.3	5.7×10^{-5}	0.0	2.087	.0014
54-1001	141.5	1.20	15.6	48.2	32.4	8.2×10^{-5}	0.0	1.429	.0037
54-1002	142.5	1.19	11.5	49.1	23.4	2.5×10^{-5}	1.7	1.393	.0154

Tshirege Member, Unit 1a									
Borehole	Depth (ft)	ρ_b (g/cm^3)	θ (vol. %)	Porosity (%)	Saturation (%)	K_{SAT} (cm/sec)	θ_r (%)	N	α
CDBM-1	23.5	1.17	2.7	48.8	5.5	6.2×10^{-5}	0.0	1.939	.0029
CDBM-1	34.0	1.07	5.8	46.2	12.7	2.2×10^{-4}	0.0	1.634	.0055
CDBM-2	38.0	0.94	8.3	48.4	17.2	4.5×10^{-4}	2.6	1.791	.0071
CDBM-1	44.0	1.26	9.3	44.5	20.8	7.0×10^{-5}	0.0	1.682	.0041
CDBM-1	54.0	1.09	8.9	44.6	20.1	4.6×10^{-4}	0.0	1.519	.0070
CDBM-1	64.0	1.23	11.2	45.1	24.9	1.2×10^{-4}	0.5	1.724	.0053
LLM 85-06	115	—	—	56.3	—	9.1×10^{-5}	—	—	—
LLM 85-11	115	—	—	60.1	—	1.8×10^{-4}	—	—	—
LLM-85-05	123	—	—	65.6	—	1.6×10^{-4}	—	—	—
LLM-85-01	124	—	—	48.9	—	2.2×10^{-4}	—	—	—
54-1003	156.0	1.14	4.9	43.2	11.3	1.3×10^{-4}	2.5	1.765	.0040
54-1006	160.5	1.13	1.8	52.6	3.4	1.2×10^{-4}	—	—	—
54-1002	178.5	1.16	6.6	39.3	16.8	6.5×10^{-5}	0.0	1.815	.0043
54-1003	206.0	1.18	8.0	42.8	18.7	1.5×10^{-4}	—	—	—
54-1002	243.5	1.14	27.0	39.3	19.1	1.7×10^{-4}	0.0	1.745	.0062
54-1003	260.5	1.11	9.6	48.8	19.7	2.7×10^{-4}	—	—	—
54-1003	270.5	1.31	12.1	41.0	29.5	2.6×10^{-4}	—	—	—

* Moisture content (θ) estimated from moisture profiles in Kearl et al. (1986a, b).

TABLE 1 (concluded)

Borehole	Depth (ft)	ρ_b (g/cm^3)	θ (vol. %)	Porosity (%)	Saturation (%)	K_{SAT} (cm/sec)	θ_r (%)	N	α
Tsankawi/Cerro Toledo									
CDBM-1	89.0	1.20	17.6	44.3	39.9	2.3×10^{-4}	0.0	1.428	.0131
CDBM-1	94.0	1.05	10.4	50.3	20.8	1.5×10^{-3}	1.6	1.585	.0173
Otowi Member									
Borehole	Depth (ft)	ρ_b (g/cm^3)	θ (vol. %)	Porosity (%)	Saturation (%)	K_{SAT} (cm/sec)	θ_r (%)	N	α
CDBM-2	66.5	1.16	11.6	44.6	26.1	5.0×10^{-4}	1.7	1.598	.0084
CDBM-2	67.5	1.22	12.3	44.0	27.9	2.7×10^{-4}	3.9	1.987	.0060
CDBM-1	104.0	1.20	15.1	44.6	33.8	2.3×10^{-4}	0.0	1.489	.0064
CDBM-1	114.0	1.29	15.6	45.1	34.6	1.6×10^{-4}	2.5	1.778	.0045
CDBM-1	124.0	1.10	11.0	43.7	25.1	2.9×10^{-4}	0.0	1.447	.0082
CDBM-1	134.0	1.24	11.7	44.7	26.2	1.6×10^{-4}	1.2	1.646	.0057
CDBM-1	144.0	1.14	10.2	42.8	23.9	4.2×10^{-4}	4.2	2.307	.0055
CDBM-1	154.0	1.29	11.1	41.0	27.1	1.0×10^{-4}	2.7	1.890	.0039
CDBM-1	164.0	1.21	10.6	43.6	24.2	1.7×10^{-4}	0.0	1.485	.0061
CDBM-1	174.0	1.18	10.1	41.2	24.4	2.1×10^{-4}	3.0	1.897	.0053
CDBM-1	184.0	1.18	9.3	43.2	21.4	3.0×10^{-4}	2.6	1.894	.0062
CDBM-1	189.0	1.19	9.4	43.0	21.9	1.8×10^{-4}	0.8	1.648	.0057

The laboratory method for determining characteristic curves involves the measurement of θ at discrete values of ψ, while for most purposes, some sort of continuous function [either $\theta(\psi)$ or $\psi(\theta)$] is desired. Various curve-fitting functions have been proposed, ranging from simple power-law fits to more complex multiparameter models. One multiparameter model that has met with wide acceptance is the van Genuchten curve (van Genuchten et al. 1980), given by the following function:

$$\tilde{\theta} = \frac{\theta - \theta_r}{\theta_s - \theta_r} = \frac{1}{\left[1 + |\alpha\psi|^N\right]^M} , \qquad (1)$$

where $\tilde{\theta}$ = effective saturation,
θ = moisture content (cm^3/cm^3),
θ_r = residual moisture content,
θ_s = saturated moisture content (porosity),

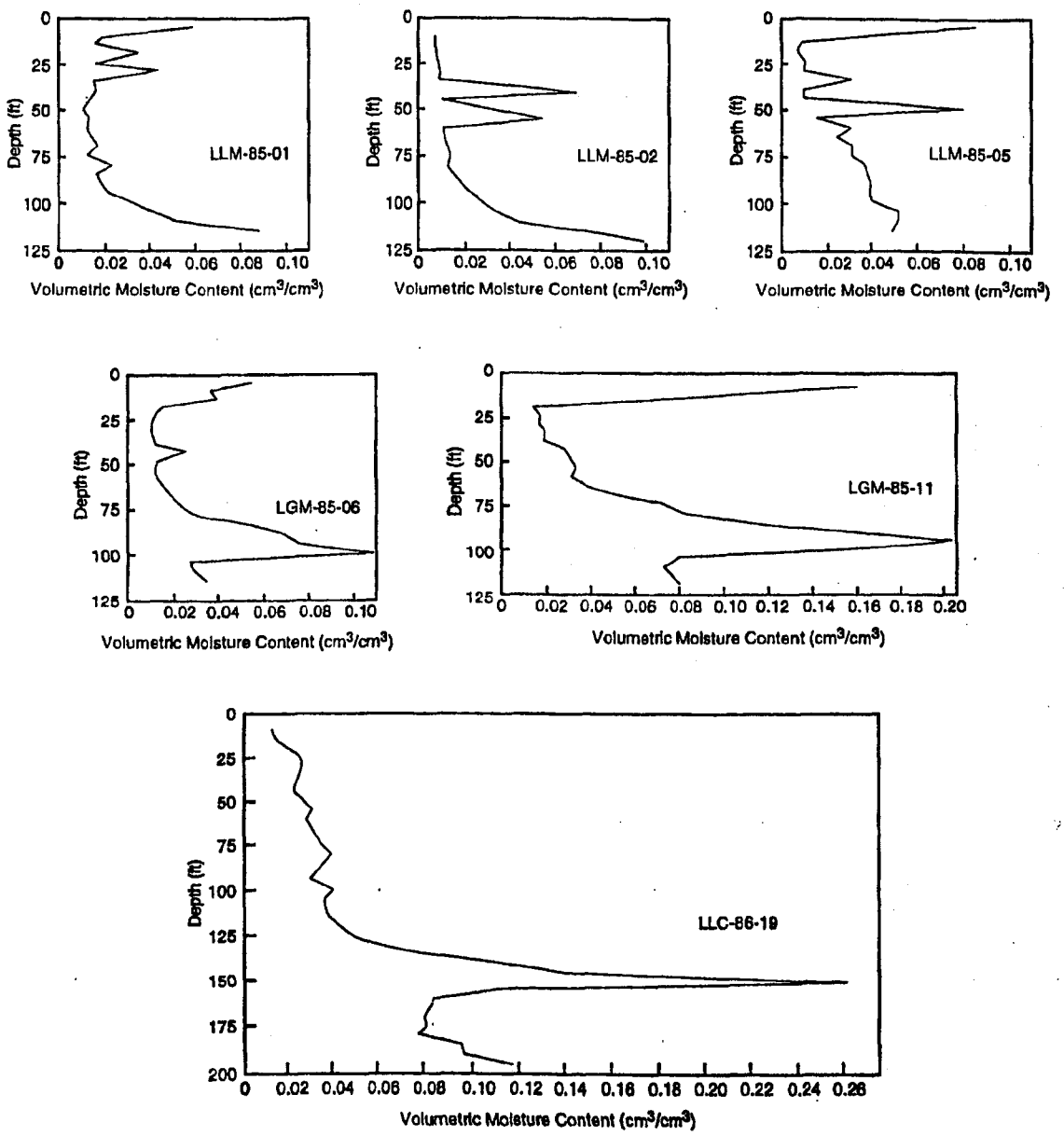

Figure 8. Volumetric moisture vs. depth for 12 boreholes (Kearl et al. 1986a,b).

ψ = matric suction,
α, N = van Genuchten fitting parameters, and
$M = 1\text{-}1/N$.

The van Genuchten curve is fit to the measured data by varying the two parameters, α and N.

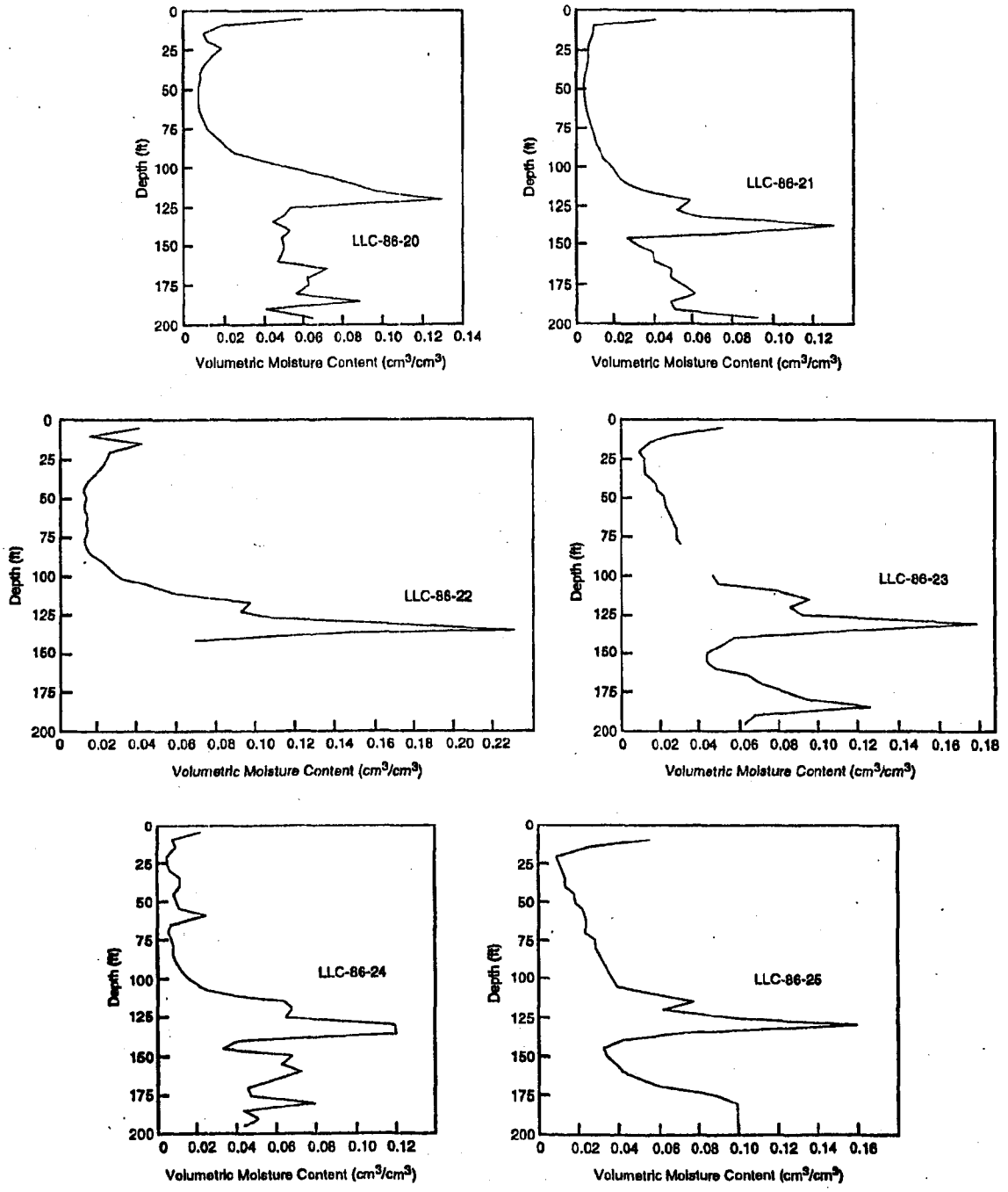

Figure 8 (concluded). Volumetric moisture vs. depth for 12 boreholes (Kearl et al. 1986a,b).

TABLE 2
PRESSURE HEAD VS. MOISTURE DATA FROM LISTED SOURCES[a]

54-1001, 67.8[b] Pressure Head (-cm water)	Moisture (vol. %)	54-1001, 82.5 Pressure Head (-cm water)	Moisture (vol. %)	54-1001, 101.5 Pressure Head (-cm water)	Moisture (vol. %)
0.1	41.4	0.1	46	0.1	51.4
51	38.6	51	43.3	51	46.8
112	37.3	112	41.3	112	44.1
326	29.3	326	38.1	326	37.3
918	25.7	918	35.1	918	21.4
6884	1.3	4304	2	6333	1.9
18101	1.2	14012	1.1	12656	1.2

54-1001, 121.5 Pressure Head (-cm water)	Moisture (vol. %)	54-1001, 141.5 Pressure Head (-cm water)	Moisture (vol. %)	54-1002, 91.8 Pressure Head (-cm water)	Moisture (vol. %)
0.1	46.4	0.1	48.2	0.1	46
51	42.4	51	44.6	51	43.6
99	40.4	112	43.1	112	42.4
306	34.6	326	37.7	311	38.4
920	21.7	918	28.8	903	32.3
5304	6.5	5599	11.2	5915	2.1
12074	3.8	21283	7.8	17948	0.7

54-1002, 121.5 Pressure Head (-cm water)	Moisture (vol. %)	54-1002, 142.0 Pressure Head (-cm water)	Moisture (vol. %)	54-1002, 178.5 Pressure Head (-cm water)	Moisture (vol. %)
0.1	49.5	0.1	49.1	0.1	39.3
51	45.3	61	43.6	51	37.7
112	43.6	102	33.9	102	35.2
311	37.4	301	27.8	306	25.9
903	22.5	923	26.6	918	20.9
6884	1.9	7118	9	5721	2
20886	1.2	17071	7	25495	1.6

a. Stephens and Associates 1991, Stephens and Associates 1992b, Stephens and Associates 1994a
b. Hole designation, sample depth (ft)

TABLE 2 (continued)

54-1002, 243.5		54-1003, 101.5		54-1003, 156.0	
Pressure Head (-cm water)	Moisture (vol. %)	Pressure Head (-cm water)	Moisture (vol. %)	Pressure Head (-cm water)	Moisture (vol. %)
0.1	39.3	0.1	51	0.1	43.2
51	37.3	51	46.1	51	41.7
102	33.1	112	44.4	102	40
306	22	311	37.8	306	30.2
918	20.7	903	27.7	918	28.1
5283	2.2	5599	1.7	7169	5.3
14094	1.9	27769	0.7	14818	4.6

54-1006, 41.5		54-1006, 76.2		54-1006, 124.0	
Pressure Head (-cm water)	Moisture (vol. %)	Pressure Head (-cm water)	Moisture (vol. %)	Pressure Head (-cm water)	Moisture (vol. %)
0.1	44.9	0.1	44.5	0.1	43.5
51	40.8	51	42.1	51	39.8
102	38.5	112	40.9	102	38.7
296	24.8	311	34.4	296	33.3
918	15.5	903	29.3	923	20.5
7536	2	6098	2.5	6557	3.8
13257	1.1	21630	0.9	14104	2.2

54-1006, 136.0		54-1006, 160.5		8LLC85-14, 29.0	
Pressure Head (-cm water)	Moisture (vol. %)	Pressure Head (-cm water)	Moisture (vol. %)	Pressure Head (-cm water)	Moisture (vol. %)
0.1	47.2	0.1	52.6	0.1	44.1
51	45.3	51	42.3	53	39.6
112	44.3	102	40.5	104	38.1
311	40.7	306	34	512	16.1
903	29.8	918	32	1030	8.2
4691	4	6853	0.8	3040	2.8
14746	1.9	13961	0.9	5080	1.4
—	—	—	—	15200	1

TABLE 2 (continued)

5LLC85-15, 10.0		2ALLC8622, 55.0		2BLLC8622, 55.0	
Pressure Head (-cm water)	Moisture (vol. %)	Pressure Head (-cm water)	Moisture (vol. %)	Pressure Head (-cm water)	Moisture (vol. %)
0.1	48.2	0.1	51	0.1	48.3
0.1	46.4	53	49.3	53	45.8
53	48.2	104	48.5	104	43.3
104	39.1	512	21.8	512	21.3
512	16.6	1030	11.1	1030	10.4
1030	10.1	3040	4.7	3040	4.1
3040	5.8	5080	3.1	5080	2.8
5080	5.1	15200	2.3	15200	0.1
15200	4.1	—	—	—	—

7LLC8622, 65.0		1LLC8622, 132.0		1BLLC8622, 132.0	
Pressure Head (-cm water)	Moisture (vol. %)	Pressure Head (-cm water)	Moisture (vol. %)	Pressure Head (-cm water)	Moisture (vol. %)
0.1	48.7	0.1	50.7	0.1	50.8
53	47.7	53	49.7	53	50.9
104	46.1	104	48.3	104	49.9
512	27	512	37.7	512	37.1
1030	11.6	1030	31.8	1030	30.9
3040	3.4	3040	17.1	3040	16.6
5080	1.4	5080	12.1	5080	11.7
15200	0.7	15200	8.7	15200	9.3

CDBM1, 23.5		CDBM1, 34.0		CDBM1, 44.0	
Pressure Head (-cm water)	Moisture (vol. %)	Pressure Head (-cm water)	Moisture (vol. %)	Pressure Head (-cm water)	Moisture (vol. %)
0.1	48.82	0.1	46.18	0.1	44.53
34	47.59	31	44.7	31	43.68
111	44.59	107	40.5	107	41.44
308	35.54	306	27.84	306	30.77
714	24.26	714	20.68	714	19.25
2295	21.33	1632	18.8	1632	13.94
5303	18.35	4875	16.96	4875	11.26
15348	14.8	15909	15.93	15909	10.06
2917	3.63	3885	4.99	5354	4.43
6200	3.07	11208	3.3	14400	2.49
19519	2.1	22517	2.56	—	—

TABLE 2 (continued)

CDBM1, 54.0		CDBM1, 64.0		CDBM, 89.0	
Pressure Head (-cm water)	Moisture (vol. %)	Pressure Head (-cm water)	Moisture (vol. %)	Pressure Head (-cm water)	Moisture (vol. %)
0.1	44.6	0.1	45.12	0.1	44.25
34	42.43	31	43.42	68	35.91
111	37.31	107	39.53	134	30.96
308	25.24	306	27.41	207	26.56
714	22.51	714	17.3	301	25.71
2295	20.49	1632	14.26	707	22.26
5303	18.81	4875	11.69	1448	19.74
15348	16.3	15909	10.79	5252	17.12
4120	5.6	4304	4.25	15042	13.09
18428	3.09	20212	2.64	2774	7.79
—	—	—	—	7791	6.04
—	—	—	—	20835	4.89

CDBM1, 94.0		CDBM1, 104.0		CDBM1, 114.0	
Pressure Head (-cm water)	Moisture (vol. %)	Pressure Head (-cm water)	Moisture (vol. %)	Pressure Head (-cm water)	Moisture (vol. %)
0.1	50.25	0.1	44.58	0.1	45.08
31	44.11	69	41.39	31	43.61
107	32.6	136	37.39	107	40.27
306	18.93	208	31.4	306	30.52
714	16.59	301	29.27	714	18.38
1632	15.59	707	21.31	1632	14.15
4875	13.15	1448	18.53	4875	11.49
15909	12.21	5252	17.21	15909	10.4
5792	4.94	15042	15.47	4171	6.83
24118	3.06	7506	6.07	15746	4.23
—	—	20743	4.43	—	—

TABLE 2 (continued)

CDBM1, 124.0		CDBM1, 134.0		CDBM1, 144.0	
Pressure Head (-cm water)	Moisture (vol. %)	Pressure Head (-cm water)	Moisture (vol. %)	Pressure Head (-cm water)	Moisture (vol. %)
0.1	43.73	0.1	44.7	0.1	42.84
69	39.33	68	41.07	31	41.18
134	35.48	135	37.63	107	38.04
207	28.64	207	32.31	306	20.57
301	25.97	301	28.02	714	18.63
707	22.46	707	18.44	1632	18.47
1448	17.97	1448	15.32	4875	18.04
5252	16.85	5252	13.98	15909	17.63
15042	13.92	15042	12.39	4395	5.37
6037	6.46	2499	6.38	19978	3.59
13359	4.68	5242	5.91	—	—
—	—	16857	3.66	—	—

CDBM1, 154.0		CDBM1, 164.0		CDBM1, 174.0	
Pressure Head (-cm water)	Moisture (vol. %)	Pressure Head (-cm water)	Moisture (vol. %)	Pressure Head (-cm water)	Moisture (vol. %)
0.1	41.03	0.1	43.56	0.1	41.22
31	39.52	68	40.27	31	40.08
107	37.23	136	37.02	107	36.6
306	28.71	209	30.55	306	23.9
714	16.68	301	27.74	714	18.77
1632	14.96	707	24.8	1632	16.64
4875	13.24	1448	22.11	4875	14.28
15909	12.37	5252	20.61	15909	13.41
4395	5.64	15042	18.31	2978	6.47
16378	3.89	5374	5.3	5711	4.7
—	—	25128	3.95	21895	3.41

TABLE 2 (concluded)

CDBM1, 183.5		CDBM1, 188.5		CDBM2, 27.5	
Pressure Head (-cm water)	Moisture (vol. %)	Pressure Head (-cm water)	Moisture (vol. %)	Pressure Head (-cm water)	Moisture (vol. %)
0.1	43.23	0.1	43	0.1	47.9
70	39.44	28.4	41.81	34	41.13
137	34.35	97	38.4	111	28.3
210	27.1	316	25.8	308	22.76
301	24.35	714	17.66	714	20.95
707	20.81	1530	16.06	2295	19.47
1448	18.07	5150	13.61	5303	18.25
5252	16.79	15297	12.26	15348	16.45
15042	14.33	7448	4.17	6608	9.65
2458	5.39	13250	3.31	19019	7.71
4151	4.67	24531	2.86	—	—
21487	3.67	—	—	—	—

CDBM2, 37.5		CDBM2, 66.5		CDBM2, 67.5	
Pressure Head (-cm water)	Moisture (vol. %)	Pressure Head (-cm water)	Moisture (vol. %)	Pressure Head (-cm water)	Moisture (vol. %)
0.1	48.39	0.1	44.56	0.1	43.97
34	45.63	34	42.12	34	42.43
111	39.58	111	36.69	111	37.72
308	24.94	308	22.13	308	23.02
714	19.53	714	17.69	714	19.02
2295	16	2295	14.22	2295	17.43
5303	11.89	5303	13.11	5303	16.38
15348	9.37	15348	11.74	15348	14.76
2580	6.77	4956	5.82	4844	5.75
4752	5.5	16847	3.91	18214	3.88
16266	3.88	—	—	—	—

Rogers and Gallaher (1994b and 1995) provide a compendium of moisture retention curve fits for the tuff core data and include data from measurements made on crushed tuff (Abeele 1979a, 1984). Mean α and N values for Bandelier Tuff core samples beneath TA-54, as compiled by Rogers and Gallaher (1994b), are listed in Table 3, along with other physical properties of tuff; the properties help constrain the performance assessment models. The software program RETC (van Genuchten et al. 1991) was used for the curve fitting. Full details of the θ-ψ measurements are contained in the original references cited above. The data and references in Table 2 are provided to enable the reader to critically evaluate the quality of the data and to use curve-fitting methods other than van Genuchten, if desired.

3.2.2.1 Tuff

Numerous characteristic curve calculations have been made for crushed Bandelier Tuff (Abeele 1979a, Abeele et al. 1981, Abeele 1984, Abeele et al. 1986) and intact core samples from beneath TA-54 (Rogers and Gallaher 1994b).

3.2.2.2 Alluvium

No characteristic curve data exist for alluvial units on the Pajarito Plateau. Alluvial cover on Mesita del Buey and MDA G is less than 1 m (3.3 ft) thick and is highly disturbed by human activity. Application of crushed tuff, asphalt roads and parking lots, cement pads and caps on shafts, heavy truck traffic on unpaved roads, and maintenance of natural or replanted vegetation have created a unique soil environment over the disposal units. Any influence on infiltration of moisture by the alluvium must be evaluated in future modeling efforts when data are available.

3.2.2.3 Pre-Bandelier Units

To date, there has been only one characteristic curve measured for units other than the Bandelier Tuff. This is a curve measured in the geotechnical laboratory (Stephens and Associates 1994b) on a basalt core sample taken from borehole SHB-1. This single curve cannot be considered in any way representative of the heterogeneous basaltic flows and flow breccias beneath TA-54.

3.2.3 Saturated Conductivity and Unsaturated Conductivity Curves

Saturated hydraulic conductivity, K_{sat}, is a measure of how readily a single fluid moves through a porous medium at saturation. Laboratory measurements are part of the typical analysis suite performed on core samples in geotechnical laboratories. Conductivity values for the stratigraphic units presented in Table 3 are taken from Stephens and Associates (1994a, 1992) and Kearl et al. (1986a, b).

The unsaturated conductivity curve relates the hydraulic conductivity of a fluid to its saturation in the system and must also be known for making numerical predictions of flow. The K-θ curve can also be used to estimate in situ infiltration rates from field moisture content measurements, given a number of simplifying assumptions. If the θ-ψ characteristic curve relationship is known, then given either the K-θ or K-ψ curve, the other can be calculated.

TABLE 3

SUMMARY OF GEOHYDROLOGIC PROPERTIES BENEATH MDA G, MESITA DEL BUEY

	Description				
Stratigraphic Unit	Unit 2b, Tshirege Member	Unit 2a, Tshirege Member	Unit 1b, Tshirege Member	Unit 1a, Tshirege Member	Tsankawi Pumice/Cerro Toledo
Thickness (typical)	12.2 m (40 ft)	13.7 m (45 ft)	7.6 m (25 ft)	15.2 m (50 ft)	Tsankawi: 1.8 m (6 ft); Cerro Toledo: 5 m (16 ft)
Lithology Summary (aft: ash-flow tuff)	Massive crystal-rich slightly welded aft, devitrified, vapor-phase altered, local pumice swarms, thin (0.2 m) basal surge	Massive crystal-rich nonwelded aft, devitrified, pumice-rich, gray-brown crystal-rich lapilli (>12% by vol.)	Massive crystal-rich nonwelded aft, devitrified, pumice-rich, brown crystal-rich lapilli (>12% by vol.), local pumice swarms, ash falls	Massive nonwelded nonindurated aft, vitric, pumice-rich, pumice are silky and vitreous, crystal-rich lapilli	Tsankawi: Massive air-fall tuff of 1-10 cm white pumice lapilli, 0.3-m surge bed of crystals and ash on top. Cerro Toledo: Moderately bedded, medium- to fine-grained tuffaceous sandstone and siltstone, moderately to poorly sorted.
Fracture Spacing	1.0-1.3 m, fractures continuous into upper Unit 1v	1.0-1.3 m (upper 3 m), *fewer* fractures deeper	No data, few fractures observed in outcrop	No data, few fractures observed in outcrop	No data, rare fractures in outcrop
Fracture Dip and Aperature	87° median, 3 mm median (3.1 ± 2.1 mm), max 13 mm	84° median, 3 mm median (5.3 ± 11.1 mm), max 100 mm	No data, assumed vertical fractures	No data, assumed vertical fractures	No data, assumed vertical fractures
Fracture Fill (XRD)	72% are filled, 9% plated, 19% open. Feldspar> trid-Q-crist> calcite>> gyp, hematite. Smectite> feldspar-Q-trid-crist>calcite	82% are filled or plated with brown clays. 18% are open. No caliche fracture-fill observed in this unit.	No data	No data	No data
Density (g/cm^3) - median - mean	1.37 1.37±.09 (n = 3)	1.26 1.24±.03 (n = 9)	1.20 1.18±.08 (n = 9)	1.14 1.15±0.09 (n = 13)	1.12 1.12±.10 (n = 2)
Porosity (%) -median - mean	45.7 48.1±9.33 (n = 12)	48.7 51.7±9.53 (n = 13)	49.3 50.9±5.80 (n = 12)	46.2 48.0±7.22 (n = 17)	47.3 47.3±4.24 (n = 2)
Vol. moisture (%) -median - mean	2.00 2.57±1.91 (n = 3)	1.50 1.89±0.95 (n = 13)	10.0 10.88±6.20 (n = 12)	8.3 8.94±6.22 (n = 13)	14.0 14.00±5.09 (n = 2)
K_{sat} (cm/s) - median - mean	4.15×10^{-4} 4.37×10^{-4} $\pm4.02\times10^{-4}$ (n = 12)	1.30×10^{-4} 1.48×10^{-4} $\pm6.59\times10^{-5}$ (n = 13)	5.15×10^{-5} 1.670×10^{-4} $\pm3.60\times10^{-4}$ (n = 12)	1.60×10^{-4} 1.88×10^{-4} $\pm1.19\times10^{-5}$ (n = 17)	8.65×10^{-4} 8.65×10^{-4} $\pm8.98\times10^{-4}$ (n = 2)
Saturation (%) -mean	5.7±4.29 (n = 3)	3.7±1.73 (n = 13)	21.3±12.06 (n = 12)	16.9±7.22 (n = 13)	30.3±13.50 (n = 2)
van Genuchten Fitting Parameters -median - mean	θ_r = 0.0 1.3±2.19 (n = 3)	θ_r = 0.0 0.2±0.67 (n = 9)	θ_r = 0.0 0.9±1.56 (n = 8)	θ_r = 0.0 0.6±1.11 (n = 9)	θ_r = 0.8 0.8±.1.13 (n = 2)
	α = .0060 .0061±.0002 (n = 3)	α = .0030 .0030±.0009 (n = 9)	α = .0033 .0044±.0045 (n = 8)	α = .0053 .0052±.0014 (n = 9)	α = .0152 .0152±.0030 (n = 2)
	n = 1.890 1.898±.1422 (n = 3)	n = 1.932 2.027±.2279 (n = 9)	n = 1.647 1.660±.2195 (n = 8)	n = 1.745 1.735±.1183 (n = 9)	n = 1.506 1.506±.1110 (n = 2)

TABLE 3 (concluded)

Stratigraphic Unit	Description				
	Otowi Member	Guaje Pumice	Cerros del Rio basalts	Puye Formation	Santa Fe Group
Thickness	36.6 m (120 ft)	3.7 m (12 ft)	>36.6 m (>120 ft)	~200 m (~650 ft)	>350 m
Lithology Summary (aft: ash-flow tuff)	Massive moderately crystal-rich nonwelded aft, vitric, rare pumice swarms, but may contain up to 30% pumice	Basal nonwelded pumice lapilli bed, vitric	Dense highly fractured multiple basaltic to andesitic lava flows, separated by 1-3 m thick flow breccias, interbedded with Puye Formation	Fanglomerates, conglomerates, fluviatile and debris-flow deposits, minor interbedded ash and pumice falls, interstratified basalt flows may dominate in upper half, includes 20 m of coarse poorly consolidated basal conglomerate (Totavi Lentil)	Fluvial sandstones, siltstones, conglomerates, with subordinate eolian and lacustrine deposits, and ash beds; interbedded basalt flows and breccias constitute 15-45% of the group beneath Mesita del Buey
Fracture Spacing	No data, few fractures observed in outcrop	No data, rare fractures observed in outcrop	No data, ~ 0.3 m estimated from outcrops	No data, poor fracture development in outcrops	No data
Fracture Dip and Aperature	No data	No data	No data, ~ 5 mm estimated from outcrops	No data	No data
Fracture Fill (XRD)	No data, some filled with caliche in outcrops	No data	None	No data	No data
Density (g/cm^3) - median - mean	1.20 1.20±.056 (n = 12)	No data	No data, estimated 2.4-3.1	No data	No data
Porosity(%) -median - mean	43.6 43.5±1.32 (n = 12)	No data	No data	No data	No data
Vol. Moisture (%) - mean	11.50±2.01 (n = 12)	No data	No data	No data	No data
K_{sat} (cm/s) - median - mean	2.20×10^{-4} 2.49×10^{-4} $\pm 1.16 \times 10^{-4}$ (n = 12)	No data	No data	No data	No data
Saturation (%)	26.4±4.12 (n = 12)	No data	No data	No data	No data
van Genuchten Fitting Parameters (θ_r, α, n)	θ_r = 2.1 1.88±1.49 (n = 12) α = .0059 .0060±.0009 (n = 12)) n = 1.713 1.755±.2528 (n = 12)	No data	No data	No data	No data

In writing the governing equations for flow, the unsaturated conductivity is often factored into two terms: the saturated conductivity (K_{sat}) and the relative conductivity (or relative permeability) (K_{rel}), i.e.,

$$K_{unsat} = K_{sat} \bullet K_{rel} \ , \tag{2}$$

with $0 \leq K_{rel} \leq 1$.

Unsaturated conductivity curves can either be directly measured or can be estimated in a number of ways. Direct measurement techniques include both field and laboratory methods. Direct measurements of K_{unsat} tend to be difficult, time-consuming, and expensive and are therefore much less common than K_{sat} measurements. Examples of techniques include laboratory column and ultracentrifuge studies and field infiltrometer studies (Conca and Wright 1992).

A faster and less costly alternative to direct measurement of unsaturated hydraulic conductivity is to use a mathematical estimation technique for K_{rel} (θ). Candidate models have been proposed by Campbell (Abeele 1979b), Mualem (1976), and Burdine (van Genuchten et al. 1991). These models assume that the shape of the characteristic curve implies certain properties of the pore structure of the medium and, using characteristic curve-fitting parameters, predicts K_{rel} as a function of saturation. K_{unsat} is then computed as the product of the K_{rel} function and a measured value of K_{sat}.

$$K = K_{sat}\theta^{-1/2}\left[1-(1-\theta^{-1/M})^{M}\right]^{2} \ . \tag{3}$$

In situ field permeability measurements form another category of directly measured conductivity data. These measurements, which include downhole air permeability tests, packer tests, slug tests, and aquifer tests, all measure conductivity (or some closely related parameter) at a single field moisture content. Therefore, they do not provide information on K-θ for other values of θ, which would have to be extrapolated by some other means. They are also more difficult to perform and interpret than laboratory tests. However, these tests are the only ones that provide data on field-scale properties that reflect large-scale heterogeneities and fractures, data for relatively undisturbed materials, and the only data for soft or unconsolidated geologic intervals that are impossible to core intact.

3.2.3.1 Tuff

3.2.3.1.1 Intact Tuff

Measurements on intact tuff by the geotechnical laboratory of Daniel B. Stephens and Associates have produced numerous relative permeability curves for Bandelier Tuff at TA-54 and elsewhere on the Pajarito Plateau. These curves were produced using the van Genuchten/Mualem model (van Genuchten et al. 1991), with laboratory characteristic

curve measurements on core samples. Results are summarized by Rogers (1994) and Rogers and Gallaher (1995).

As part of the current ER Project site characterization efforts at TA-54, a number of in situ air permeability measurements have been conducted. Details of these studies are summarized in Appendix C. One of the ER Project studies included the use of borehole dual packer methods to measure in situ air permeability values in six boreholes in the proposed expansion area for MDA G. The measured air permeability values in each borehole are presented in Tables C-1 to C-6 and are summarized in Table C-7. Borehole locations are shown on Figure B-1. All of the measurements were performed with the air extraction method at an open interval of 27 in. (69 cm) between the borehole packers. The stratigraphic units tested were 2b, 2a, 1b, and 1a of the Tshirege Tuff Member; the Tsankawi pumice bed; the Cerro Toledo interval; and the Otowi Tuff Member [only one measurement (0.55 darcies) was performed]. For all measurements, air permeability values ranged between 0.35 darcies and 172.47 darcies. The highest values were measured on borehole intervals with open joints that were identified from geologic description of the continuous core.

The greatest range in air permeability values was measured in Unit 1b (0.63–172.47 darcies). The low values are believed to reflect the low air permeability of the matrix while the high values are due to measurements on open joints. Air permeabilities measured in the central and lower section of Unit 1a were low, with a median value of 1.12 darcies (Table C-7). The Otowi Tuff is also believed to have low air permeability; a low value of 0.55 darcies was measured in the one straddle packer test performed in this stratigraphic unit.

Laboratory measurements of air permeability were conducted on core from four of the six boreholes where straddle packer measurements were performed (Table C-8). In general, the core measurements determined lower air permeability than the colocated straddle packer measurements. This is expected because the laboratory measurements were on unfractured 6-in. (15-cm) lengths of core whereas the straddle packer measurements were on 27-in. (69-cm) borehole intervals where features such as open joints, fractures, or changes in rock matrix could influence the measurement results.

3.2.3.1.2 Crushed Tuff

Crushed Bandelier Tuff has historically been used for lining new disposal pits to a depth of about 0.3 m (13.0 in.), for separating some disposed of containers within the pits, and for covering pits. Stephens and Associates (1994b) provide one analysis of the hydraulic properties of a crushed Bandelier Tuff sample; the method of analysis was the pressure-plate and thermocouple psychrometer. The following values were reported: density was 1.40 g/cm^3, initial moisture content was 7.5 vol.%, θ_{sat} equaled 38.3%, and saturation equaled 19.6%. Using Equations (1, 2, and 3) for curve fit to the retention data, van Genuchten parameters are α equals .0083 and N equals 1.779, with a residual saturation calculated at 0.0%. K_{sat} for this single sample is 8.2 x 10^{-4} cm/sec. Calculated unsaturated conductivity for moisture ranging from 10% to 20% apparently vary from 10^{-8} to 10^{-6} cm/sec (Rogers and Gallaher 1995).

3.2.3.2 Alluvium

Local hydraulic information on alluvial aquifer materials comes from slug tests. These are single-well aquifer tests that provide only gross, and sometimes inaccurate, K_{sat} estimates. One set of slug tests has been conducted for the alluvial aquifer in Pajarito Canyon (Los Alamos Technical Associates 1991). These tests show K_{sat} ranging between 4.2 x 10^{-6} and 1.2 x 10^{-5} cm/sec (0.012 and 0.035 ft/day). These numbers are surprisingly low, much lower than the results of nine slug tests in Los Alamos Canyon alluvium that indicated a range of 1.5 x 10^{-3} to 4.0 x 10^{-2} cm/sec (4.8 x 10^{-5} ft/sec to 1.3 x 10^{-3} ft/sec) with an average of 1.4 x 10^{-2} cm/sec (4.7 x 10^{-4} ft/sec) (LANL 1993). The Environmental Surveillance Group has also conducted slug tests of the alluvial aquifer in Mortandad Canyon, but results have not been finalized or released (D. B. Rogers, personal communication, 1995).

3.2.3.3 Pre-Bandelier Tuff Units

The only available hydrologic data on the pre-Bandelier units of the Pajarito Plateau consist of estimates of saturated conductivity within the regional aquifer; these data were derived from specific capacity tests in production wells and test wells. These data, summarized by Purtymun (1984) (Table 4), are limited to good production zones; less permeable units, such as massive parts of the Cerros del Rio basalts, are not represented.

TABLE 4
SATURATED CONDUCTIVITY VALUES FOR PRE-BANDELIER TUFF UNITS

Unit		Saturated Hydraulic Conductivity (gpd/ft^2)	(cm/sec)
Tesuque Formation (sedimentary)	mean	5.6	2.6 x10^{-4}
	range	3–9.3	1.4–4.4 x 10^{-4}
Tesuque Formation with interbedded basalts	mean	8.2	3.9 x 10^{-4}
	range	5.3–11.3	2.5–5.3 x 10^{-4}
Tschicoma Formation (volcanic flows)	mean	19	9.0 x 10^{-4}
Mixed Tesuque Formation and Puye conglomerate	range	53–83	2.5–3.9 x 10^{-3}
Puye conglomerate*	mean	98	4.6 x 10^{-3}

* Purtymun 1984

Pumping tests done at Test Area North (TAN) at the Idaho National Engineering Laboratory (now Lockheed Idaho) provide data for saturated permeabilities within a basalt aquifer. For TAN, saturated permeabilities were 1 m/day at TAN-20, 43 m/day at TAN-18, 8 m/day at TAN-21, and 177 m/day at TAN-24A. At TAN-23, permeability was estimated at >213 m/day, but the water level could not be drawn down for a long enough time for reasonable measurement (W. Soll, personal communication, 1995). We might expect similar large ranges for saturated conditions beneath the Pajarito Plateau. Conductivities for a piece of cored basalt from borehole SHB-1 west of Mesita del Buey gave values of 3×10^{-11} and 3×10^{-9} cm/sec (Stephens and Associates 1994b).

3.2.4 Hysteresis

One physical process that is not typically characterized or measured in the laboratory is hysteresis of parameter values. Hysteresis in the θ-ψ relationship is the difference in the saturation of a fluid at a given pressure as a function of the fluid displacement history. It is caused by a change in displacement behavior of a fluid depending on whether it is by a drainage displacement (air displacing water) or an imbibition displacement (water displacing air). It is worth mentioning because it can have a significant effect on θ-ψ values, as noted for Bandelier Tuff by Abrahams (1963), but is almost always ignored because it introduces major complications into the modeling and prediction effort and requires more than double the number of experiments. Furthermore, the same hysteresis that affects the θ-ψ curve will also affect the K-ψ curve, although the K-θ relationship is inherently less hysteretic. We will also ignore hysteresis, out of necessity, because there are no data available.

3.2.5 Geohydrologic Properties of Rock Units beneath MDA G

Table 3 lists representative properties of the geologic units beneath Mesita del Buey in the region of MDA G for the purpose of modeling performance of the disposal site. There are many properties, mostly for the deeper strata, for which no relevant data exist. The uncertainties produced by these data gaps should be alleviated by investigations below our current depth of sampling. The thick interval of unsaturated rock between the relatively well-known tuff and the deep aquifer provides additional delay of radionuclide transport to the water table, but current data limits any quantification.

3.3 Hydrologic Conditions Below MDA G

The previous sections focused on hydrologic properties intrinsic to the geologic materials in the vicinity of MDA G. From these properties, we can tell how the materials might behave under a wide range of hydrologic conditions, but we can only speculate about how these materials are behaving under the disposal pits. In this section, we look at information about present conditions and processes. Both types of information are critical because together they can provide an understanding of the processes that affect flow and transport today and also predictions of the effects of the processes in the future.

3.3.1 In Situ Moisture Content

Numerous measurements, both laboratory measurements of fresh core samples and neutron probe measurements, of in situ moisture content have been conducted in and around MDA G (Kearl et al. 1986a, b; Rogers and Gallaher 1994a). The data indicate a

fairly predictable moisture profile through the different stratigraphic units of the Bandelier Tuff. Generally, field moisture content in the upper 33 m (100 ft) of tuff is less than 2% by volume in areas that are undisturbed by disposal pits and shafts, and most notably, asphalt cover. Around disturbed settings caused by disposal activities, near-surface moisture content dramatically increases above the natural background state because of a loss of plant evapotranspiration and suppression of atmospheric venting by installation of large asphalt surfaces. There is evidence that the increased moisture content may occur to depths of 15 m (50 ft) beneath disturbed areas. Appendix B describes our current data for in situ moisture content measurements.

3.3.2 Perched Aquifers

There is no evidence of extensive perched aquifers under Mesita del Buey. Gardner et al. (1993) report wet samples and equipment from the Otowi section in borehole SHB-4 in Pajarito Canyon 2.4 km (1.5 miles) northwest of MDA G. During drilling near MDA L, moist fine-grained Puye Formation was encountered directly overlying the basalts. Within the basalt, thin zones (~0.3 m, 1.0 ft) of wet basalt were observed (1) in the drill air return from the drill hole during drilling, (2) when the drill air was first turned on in the morning after being shut down overnight, and (3) as saturated zones in vesicular basalt core. The drill holes were not cored continuously. The elevations where water was observed in the basalt in borehole 54-1015 were 6278 ft (1913 m), 6260 ft (1908 m), and 6250 ft (1905 m). The elevations where water was observed in the basalt for borehole 54-1016 were 6292 ft (1918 m), 6258 ft (1907 m), 6204 ft (1891 m), and 6201 ft (1890 m). Chemical analysis of the water samples collected from the drill air was not warranted because of the impromptu collection methods. Monitor ports to collect groundwater, if present, were installed in the Tsankawi pumice bed, the Puye Formation, and selected zones in the basalt. To the present time, sampling events have not found water to be present in any of the ports. We believe that small quantities of water were trapped either soon after basalt deposition or en route toward the deep aquifer (Section 2.3.2).

3.3.3 In Situ Matric Tension

Kearl et al. (1986a, b) measured downhole matric tension profiles in two holes at TA-54 using thermocouple psychrometer arrays. Rogers and Gallaher (1994a) present laboratory-derived matric tension profiles for five wells drilled at MDA G during 1994; the cores were measured using the chilled-mirror psychrometer method. These measurements, together with measured water content, can be used to infer a direction of liquid movement based on head gradients. Based on head calculations from such measurements, Rogers and Gallaher (1994a) show that moisture is driven toward a dry, high-suction interval that is associated with the pyroclastic basal surge deposits at the base of Unit 2b. This high-suction interval is present to a degree in nearly all MDA G holes where matric tension data exists.

3.4 Areas for Further Investigation

Tables 3 and 4 indicate that much critical information is lacking about the hydrogeologic system beneath the Pajarito Plateau and below MDA G, specifically. The following are areas for further investigation.

1. There is almost no information available for pre-Bandelier Tuff lithologies, including hydrologic properties, thicknesses of basalt, and elevation of the top of the sedimentary rocks that host the regional aquifer below MDA G. A carefully cored well east of MDA G that penetrated the deep aquifer could fill in some information. When completed as a groundwater monitoring well, it would be the nearest monitoring station downgradient of the disposal units at Mesita del Buey. Aquifer testing, laboratory analysis of hydraulic properties for selected deeper stratigraphic units, and long-term monitoring activity would provide tighter control on numerical modeling and checks on aquifer integrity.
2. Little is known about fracture presence, frequency, aperture, continuity, and coatings or fillings below Unit 2a. Definitive characterization of fracture fillings and coatings is missing for all units. The available information is insufficient to determine whether fractures may be a critical flow path in the system. Characterization of this site would benefit from study of fracture coatings and fills and their material properties to augment existing data on population, aperture, and orientation. This information is most accessible from existing and future disposal pit walls.
3. Final disposition of MDA G and the other disposal areas on Mesita del Buey awaits federal and state agreement on scientific, economical, and political issues. One potential outcome is capping and stabilization of wastes in place. A pilot study in the ER Project is looking at the feasibility of large-scale atmospheric air movement through permeable geologic layers beneath disposal units. Dry atmospheric air can absorb and vent moisture from porous media, thereby decreasing the mobility of contaminants and increasing the effectiveness of natural retardation effects of the matrix. Future performance assessments might take into account the benefits of such an engineered stabilization system, particularly if a passive system can be made reliable.

4.0 GEOCHEMICAL BASELINE INFORMATION AND DATA

4.1 Introduction

The purpose of this section is to provide a review of the relevant geochemical data and information required for solute-transport calculations that will be used in the performance assessment. These data will serve as input to the mass/heat transfer model FEHM (Zyvoloski et al. 1988). Specific geochemical data used as input to FEHM include sorption isotherm models, consisting of the linear (K_D), Freundlich, modified Freundlich, and Langmuir; Henry's Law constants for liquid and vapor species; chemical rate laws using the Arrhenius equation; and solubility data for solid phases.

A detailed discussion on water/rock processes is also presented in this section. Geochemical parameters, such as pH, Eh, solution composition, mineral solubility, and presence of competing and complexing ligands, have the greatest impact on the sorption behavior of the elements of concern present in the pits. The release of radionuclides from the pits will be controlled by hydraulic flux, pore-water chemistry, mineral solubility, and sorption behavior. The following data and information are needed to verify and quantify geochemical reactions: source-term characterization (types, forms, and amounts of contaminants); source-term geochemistry (mineralogy, speciation, solubility, sorption,

pore-water chemistry, and reaction rates); and hydrogeological/geochemical characterization (mineralogy, fracture distribution, fracture mineralogy, sorption capacity of fracture material, hydraulic conductivity, porosity, and moisture content) of Bandelier Tuff and other geologic media at the site.

Very little site-specific geochemical data on sorption capacities of the Bandelier Tuff are available (Polzer et al. 1992). Parameter data for Freundlich, modified Freundlich, and Langmuir isotherms generally are not available from Yucca Mountain experiments, and application of these isotherms to the existing sorption data is not possible. Geochemical and hydrological processes influencing solute-transport processes within the Bandelier Tuff are extremely complex; therefore, site-specific data used as input to FEHM will be required to obtain the most relevant and meaningful results for the performance assessment.

4.2 Source-Term Inventory and Geochemistry

Predicting the release of radionuclides from MDA G is complex because of the variety of contaminated material disposed of in the pits and shafts. Elements of concern include americium (Am), carbon (C), cesium (Cs), cobalt (Co), neptunium (Np), strontium (Sr), plutonium (Pu), technetium (Tc), tritium (^3H), and uranium (U). This list is based on waste inventories provided by CST-14. Specific isotopes of these elements and their associated activities are provided in Table 5. Contaminated material in Pit 37 includes metal, cellulosics (cardboard), concrete, soil, and sludge. In Pit 37, most of the activity is associated with U-contaminated metal (8.16 Ci) and Pu-contaminated cellulosics (4.37 Ci). In terms of activity per volume of contaminated material, U-contaminated metal (0.0198 Ci/m^3) and Pu-contaminated sludge (0.0218 Ci/m^3) are the most abundant waste forms in this pit. Other waste forms in Pit 37, which are not included in Table 5, are irradiation sources consisting of encapsulated materials. These materials are not considered leachable and are not included in the total inventory of radionuclides listed in Table 5. A separate investigation is being conducted to quantify the amounts of radionuclides potentially migrating from the pits. Radionuclides are characterized by different leach rates, which are controlled by desorption and dissolution processes.

Cement sludge that was processed at TA-50 is disposed of in Pit 37. The sludge consists of an alkaline (pH 12) mixture containing $Si(OH)_4$ (40 wt%), $Ca(OH)_2$ (31 wt%), and $Fe(OH)_3$ (19 wt%) with varying amounts (approximately 10 wt%) of $Al(OH)_3$, $Mg(OH)_2$, NaOH and other metal hydroxides, metal sulfates, and metal chlorides. Typical activities of radionuclides in the TA-50 sludge are as follows: Pu-239/240, 1.0×10^4 pCi/g; Pu-238, 6.5×10^4 pCi/g; Am-241, 1.0×10^4 pCi/g; U-235, < 5 pCi/g; and U-234, 200 pCi/g (Terry Filer, CST-9, personal communication, July 28, 1995). The radionuclide content and activities of older TA-50 sludge is characterized by the following: Pu-239/240, 4.0×10^4 pCi/g; Pu-238, 1.0×10^4 pCi/g; and Am-241, 5.0×10^4 pCi/g (personal communication with Terry Filer, CST-9 on July 28, 1995). The chemical composition (major ion) of this hydroxide-rich sludge is representative of hydrated cement containing $Ca(OH)_2$ and $Si(OH)_4$ (Berner 1992, Krupka and Serne 1995).

TABLE 5
SUMMARY OF RADIONUCLIDE HALF-LIVES AND TOTAL ACTIVITY IN PIT 37 AT MDA G, TA-54, NOVEMBER 1994

Nuclide	Mass (g)	Half-life (yr)	Total Inventory (Ci)
^{3}H	1.24×10^{-3}	12.33	1.2×10^{1}
^{14}C	2.02	5.73×10^{3}	9.0
^{60}Co	6.64×10^{-3}	5.27	7.5
^{90}Sr	2.34×10^{-4}	29	3.3×10^{-2}
^{99}Tc	1.55×10^{-7}	2.13×10^{5}	8.2×10^{-1}
^{129}I	5.76×10^{-7}?	1.59×10^{7}	1.0×10^{-10}?
^{137}Cs	2.76×10^{-3}	30.17	2.4×10^{-1}
^{233}U	1.05×10^{-1}	1.59×10^{5}	1.0×10^{-3}
^{234}U	1.52×10^{1}	2.44×10^{5}	9.5×10^{-2}
^{235}U	1.26×10^{5}	7.04×10^{8}	2.7×10^{-1}
^{236}U	4.81×10^{-1}	2.34×10^{7}	3.1×10^{-5}
^{238}U	2.13×10^{6}	4.47×10^{9}	7.1×10^{-1}
^{237}Np	1.42×10^{-2}	2.14×10^{6}	1.0×10^{-5}, ingrowth from ^{241}Am
^{238}Pu	5.87×10^{-2}	87.74	1.0
^{239}Pu	1.42×10^{1}	2.41×10^{4}	8.7×10^{-1}
^{240}Pu	3.18×10^{-2}	6.54×10^{3}	7.2×10^{-3}
^{241}Pu	1.09×10^{-3}	14.7	1.1×10^{-1}
^{242}Pu	2.12×10^{-5}	3.76×10^{5}	8.3×10^{-8}
^{241}Am	8.95×10^{-2}	432	2.9×10^{-1}

Source: Keller, D., personal communication with P. Longmire on November 21, 1994.

A geochemical conceptual model for MDA G is shown in Figure 9. This geochemical model is based on relevant geochemical and mineralogical data and information collected from the ER Project at the Laboratory and from the Yucca Mountain Project. The key features of this model are discussed below.

1. Surface water (snowmelt, rainwater, and/or storm runoff) enters the pits. Rainwater and snowmelt will have a low total dissolved solids (TDS) content and an acidic pH because of low concentrations of bicarbonate, calcium (Ca), sodium (Na), and magnesium. Storm runoff may have a higher TDS content and near-neutral pH because of its contact with soils, sediments, asphalt, fill, and Bandelier Tuff.

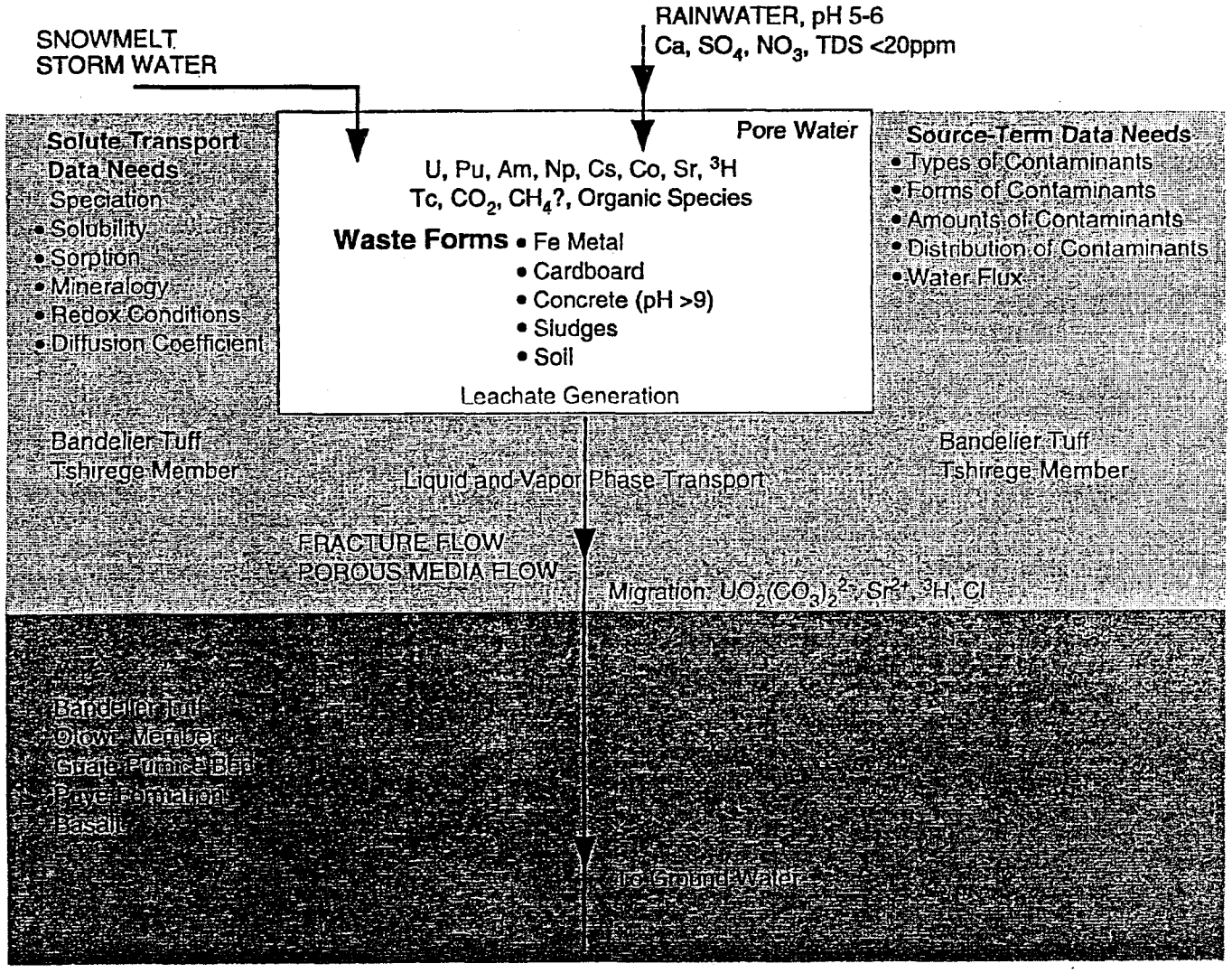

Figure 9. Geochemical conceptual model for TA-54.

2. Pore water will be generated as surface water enters the pits. This solution may approach equilibrium with crushed Bandelier Tuff, waste forms, dissolved gases, radionuclides, and other contaminants. The TDS content will increase in response to chemical reactions and pore-water residence time (mass/flux). Relatively oxidizing conditions probably prevail under unsaturated-flow conditions in areas deficient of chemical reductants, such as organic sludges, hydrogen sulfide, and methane. Localized reducing conditions are restricted to areas in the pits where reactive chemical reductants are present.

3. Important geochemical reactions controlling the release of contaminants from the pits include contaminant diffusion through waste forms, desorption of contaminants from waste forms, partial dissolution of waste forms, dissolution of contaminants, and gas generation. These geochemical reactions will be controlled by pH, Eh, speciation of contaminants, temperature, advection, and residence time of pore water. The pH may vary from near neutral to strongly alkaline values, especially if pore water comes in contact with concrete. Near-neutral pH values are expected to be dominant, however, because of the localized distribution of concrete and unsaturated-flow conditions within the pits. Contaminant leach rates will be controlled by the hydraulic flux, desorption, and equilibrium solubilities of the waste forms and contaminants.

4.3. Geochemical Transport Parameters

Release of contaminants (including radionuclides) from MDA G depends on the pit pore-water chemistry and the solubility and sorption behavior of the radionuclides. This section presents information and data derived from literature on sorption and equilibrium solubility for elements of concern at MDA G. Leach rates of radionuclides can be evaluated by considering equilibrium solubilities of solid phases containing the element of interest, e.g., U, Am, and Pu, and by determining ranges of the flux rate under unsaturated-flow conditions. Sorption values for devitrified tuff from Yucca Mountain are the primary focus of this discussion. Below MDA G, the Bandelier Tuff consists of both devitrified and vitrified rock. Other hydrogeologic units present beneath MDA G include basalts, Puye Formation, and the Santa Fe Group sediments, which are important to consider for the solute transport calculations. Unfortunately, very little hydrological and geochemical data have been collected on these strata, except for the Bandelier Tuff. Site-specific geochemical data for MDA G will make the calculations more technically defensible. Data needs are discussed in Section 4.4, Uncertainties and Future Investigations.

Distribution coefficient (K_D) values and solubility data from literature pertaining to Yucca Mountain were evaluated to estimate the potential for release of radionuclides from the pits and through the Bandelier Tuff. The Yucca Mountain experiments have relevance to MDA G because of similarities in mineralogy and sorption capacities of the Yucca Mountain tuffs and the Bandelier Tuff. The major controls of radionuclide adsorption include mineralogy and distribution of the adsorptive phases and major-ion chemistry of the solution containing the adsorbate(s). The mineralogy of devitrified volcanic tuffs at Yucca Mountain (Wolfsberg 1980) is similar to the bulk mineralogy of the Bandelier Tuff (Broxton et al. 1995). The Bandelier Tuff consists of devitrified and vitrified rock, which is assumed to have similar sorption capacities as Yucca Mountain tuffs for elements of concern based on similarities of bulk surface areas for devitrified and vitrified tuff. The dominant minerals

occurring in the devitrified tuff at Yucca Mountain include quartz, cristobalite, and feldspars with less than 5 wt% clay minerals and zeolites (Wolfsberg 1980). Devitrified sections of the Bandelier Tuff (Tshirege Member) are characterized dominantly by feldspar and quartz with some cristobalite and tridimite (Broxton et al. 1995). Clay minerals compose less than 2 wt% of the Tshirege Member (Broxton et al. 1995).

The groundwater chemistry of well J-13 at Yucca Mountain (Thomas 1987) is similar to the Water Canyon Gallery groundwater at Los Alamos (Table 6). There are some important differences, however, in temperature and major-ion chemistry, which may influence adsorption processes. The temperature of the J-13 groundwater (31.0°C) is higher than the temperature of the Water Canyon Gallery groundwater (11.3°C). The dominant cations and anions in both groundwaters are Na, calcium, and bicarbonate. The higher bicarbonate concentration in the J-13 groundwater probably accounts for the limited extent of adsorption of uranyl [U(VI)] species onto the Yucca Mountain tuffs. K_D values for U determined by Triay et al. (1994) under oxidizing conditions are less than 2 ml/g. The TDS content of the J-13 groundwater is higher than the TDS content of the Water Canyon Gallery groundwater by approximately a factor of 1.7. The J-13 groundwater may have a longer residence time within the tuff(s), which may account for the higher TDS content. The pH values for the Water Canyon Gallery and J-13 groundwaters are 7.6 and 6.9, respectively.

The geochemistry of soils is relevant to the migration of radionuclides in surface and near-surface environments at TA-54. Soils present on the Pajarito Plateau have extremely variable physical and chemical properties, including particle size, percent calcium carbonate, clay mineralogy, iron oxides, and trace element chemistry (Longmire et al. 1995). These properties influence the adsorption of potential contaminants that may be released to soils. Variations of element concentrations in soils are related to climate, topography, and to the parent materials, which include alluvial fans, sheet wash material, colluvium, wind-blown sediment, El Cajete pumice, and the Bandelier Tuff. Soils have higher concentrations of aluminum (Al), arsenic (As), barium (Ba), Ca, Cs, Co, chromium (Cr), and iron (Fe) than Bandelier Tuff samples because of the soil's higher sorptive capacity (Longmire et al. 1995). Bandelier Tuff has higher concentrations of beryllium (Be), lead (Pb), Na, potassium (K), thorium (Th), and U than the soils because of element partitioning during eruptive episodes.

A well-developed B horizon is a dominant characteristic of well-developed soil profiles. The B horizon contains a greater abundance of clay minerals and iron oxides than the A and C horizons. Clay minerals and iron oxides have relatively high surface areas that increase the adsorption capacity of a well-developed B horizon for trace elements. The B horizon contains higher concentrations of trace elements compared with A and C horizons. Distributions of the trace elements Th and U in soil horizons and in the Bandelier Tuff suggest that there has been little migration of these two elements from the soils.

TABLE 6

ANALYTICAL RESULTS OF WATER CANYON GALLERY GROUNDWATER, LOS ALAMOS, NEW MEXICO, AND WELL J-13 GROUNDWATER, YUCCA MOUNTAIN, NEVADA[a]

Element/Parameter	Water Canyon Gallery	Well J-13
Temperature (C)	11.3	31.0
pH (field)	7.6	6.9
Total dissolved solids	106[b]	278
Al	0.2[b]	0.03[b]
Ca	6.94[b]	11.5[b]
Cl	0.69[b]	6.4[b]
F	0.06[b]	2.1[b]
Fe	0.05[b]	0.04[b]
HCO_3	44.6[b]	124[b]
K	1.79[b]	5.3[b]
Mg	2.79[b]	1.76[b]
Na	4.9[b]	45[b]
NO_3 (N)	0.98[b]	0.23[b]
SiO_2	39.8[b]	64[b]
SO_4	2.85[b]	18.1[b]

a. Groundwater chemistry of Well J-13 is summarized by Thomas (1987). Input data for model simulations (speciation and mineral saturation index calculations) are described in the text using results of chemical analyses from Water Canyon Gallery, Los Alamos, New Mexico.

b. Concentration units reported in mg solute per kilogram water.

4.3.1 Element-Radionuclide Adsorption Behavior

Radionuclide-contaminated waste present in pits occurs as metals, cellulosics (cardboard), concrete, soil, and sludge. We assume that all radionuclides will be released from the waste forms and that partial sorption will only occur onto surfaces of pit fill material, Bandelier Tuff, and other hydrogeologic media. This assumption is applied to the geochemical-solute transport modeling because there is no site-specific data relevant to waste form radionuclide chemistry. In reality, some amount of each radionuclide will remain within or adsorbed onto waste-form surfaces.

Numerous batch and column adsorption studies of elements of concern and their associated radionuclides onto volcanic tuff have been performed at Yucca Mountain (Triay

et al. 1994, Wolfsberg 1980, Thomas 1987, Nitsche et al. 1993, Fuentes et al. 1987). Results of these investigations were used to select average values for batch K_D measurements, assuming that the Bandelier Tuff is the only reactive medium. Batch K_D or R_D values for Am, Cs, Np, Pu, Sr, Tc, and U were experimentally determined by Triay et al. (1994) and Wolfsberg (1980) using the following equation.

$$K_D = \frac{\text{moles or activity of radionuclide per g of solid phase}}{\text{moles or activity of radionuclide per ml of solution}} \quad . \qquad (4)$$

Other K_D values were selected from other literature references.

The dimensions for Equation (4) are $[M/M/M/L^3]$ or $[L^3/M]$, and the units of Equation (4) used in this report are ml/g or cm^3/g. R_D is the same as K_D, except that no approach to equilibrium is assumed. Average K_D values for the different elements are summarized in Table 7. Wolfsberg (1980) points out that, in an equilibrium situation, identical values for sorption should be obtained for all conditions intermediate between all activity initially on the solid (desorption) and all activity initially in solution (sorption). Wide ranges of sorption values for Cs and Sr are summarized in Wolfsberg (1980). Sorptive properties of the tuff vary with the abundance and composition of primary and secondary minerals, glass, and lithic fragments. Ranges of selected K_D values for Cs, Np, Sr, Pu, and U measured on devitrified tuff (Yucca Mountain) are summarized in Table 8.

Rundberg (1987) reports that Cs and Sr adsorb onto Yucca Mountain tuffs with moderately high K_D values and rapid kinetics. This suggests that the sorption kinetics for Cs and Sr are sufficiently fast so that equilibrium is reached for the retardation of these two elements under groundwater-flow velocities that would be reasonable for solute-transport simulations (Rundberg 1987). Rate constants for these two elements were high (for Cs, κ_1 ranged between 5.9×10^{-2} and $4.0 \times 10^{-1} s^{-1}$ and κ_2 ranged between 4.2×10^{-5} and $1.4 \times 10^{-4} s^{-1}$; for Sr, κ_1 ranged between 1.1×10^{-3} and $9.5 \times 10^{-3} s^{-1}$ and κ_2 ranged between 6.7×10^{-6} and $2.0 \times 10^{-5} s^{-1}$). The parameters, κ_1 and κ_2, are the rate constants of forward and backward reactions, respectively. The time-dependent sorption data suggest a two-step diffusional model, where diffusion inside the intracrystalline channels of zeolites and clay minerals proceeds much more slowly than does diffusion in the intercrystalline pore space (Rundberg 1987). The adsorption process at mineral surfaces, however, was rapid in the experiments simulating porous-media flow. However, the kinetics of adsorption under fracture-flow conditions are not well understood.

The actinides, specifically Pu, exhibit a slow time dependence for adsorption (Rundberg 1987). This effect is shown in Table 8, where the desorption K_D values for Am, Pu, and U are within a factor of 17 (greater than the adsorption K_D values for these elements). Rate constants κ_1 (6.37 x 10-7 s^{-1}) and κ_2 (6.37 x 10-9 s^{-1}) for Pu are smaller than the rate constants for Cs and Sr (Rundberg 1987). These higher desorption K_D values, however, may be reflective of mineral precipitation in addition to sorption reactions.

TABLE 7

AVERAGE SORPTION RATIO, K_D OR R_D (ML/G), FOR VOLCANIC ROCK, YUCCA MOUNTAIN TUFFS, OXIDIZING CONDITIONS, PH 7, 25°C

Element	Devitrified Tuff
Actinium[a]	130
Aluminum[a]	130
Americium[b]	130
Barium[b]	946
Cadmium[c]	80
Californium[a]	130
Carbon[d]	0
Chlorine[d]	0
Cesium[b]	428
Cobalt[e]	0.45
Curium[d]	50
Europium[d]	50
Gadolinium[d]	50
Hafnium[f]	500
Hydrogen (Tritium)[d]	0
Iodine[d]	0
Lead[d]	25
Molydenum[d]	4
Nickel[d]	50
Niobium[d]	100
Palladium[d]	50

a. K_Ds are estimated based on chemical similarities between americium (III) and californium (III), americium (III) and aluminum (III), and americium(III) and actinium (III).
b. Wolfsberg 1980
c. Thibault et al. 1990
d. Brookins 1984
e. Polzer et al. 1985
f. Hafnium (IV) is chemically similar to Zr (IV).

TABLE 7 (concluded)

Element	Devitrified Tuff
Plutonium[b]	110
Potassium[c]	15
Protactinium[d]	100
Radium[d]	200
Samarium[d]	50
Selenium[d]	2
Silicon[c]	35
Silver[c]	90
Strontium[b]	116
Neptunium[g]	0.007
Technetium[b]	0.3
Thorium[d]	500
Tin[d]	50
Uranium[b]	1.8
Zirconium[d]	500

b. Wolfsberg 1980
g. Triay et al. 1994
d. Brookins 1984
c. Thibault et al. 1990

The K_D values selected for the Bandelier Tuff (Table 7) represent a conservative set of values for soils forming on the Pajarito Plateau. The soils will have a higher sorptive capacity than the Bandelier Tuff for most of the elements of concern. This is because a higher abundance of geochemically active phases (clay minerals, ferric oxyhydroxide, calcium carbonate, and solid organic matter) is present in well-developed soils found at TA-54 (Davenport 1993) and throughout the Laboratory. In addition, soils have higher surface areas than the Bandelier Tuff, which enhances adsorption processes (Longmire et al. 1995).

Geochemical data for cement were provided by Bradbury and Sarott (1995) for source-term and transport analyses; the data consisted of K_D values for radionuclides measured under oxidizing conditions. These K_D values (Table 9) are the most current and critically reviewed data available from literature. Site-specific adsorption data for cement are not available for TA-54. The K_D values listed in Table 9 represent equilibrium values where

the contaminant has had adequate time to diffuse into all available internal surfaces of the fine-grained hydration gel minerals and related reaction products, such as silica and carbonate phases. These phases may be present within local alkaline conditions that may occur at the interface between alkaline sludge and the pore solution within the unsaturated zone.

TABLE 8

SORPTION AND DESORPTION RATIOS, K_D OR R_D, (ML/G) FOR VOLCANIC ROCK, YUCCA MOUNTAIN TUFFS

Element	Devitrified Tuff (Sorption)
Americium[a]	130
Cesium[a]	150–870
Neptunium[b]	0–3
Plutonium[a]	110
Strontium[a]	53–190
Uranium[a]	1.6–2.2

Element	Devitrified Tuff (Desorption)
Americium[a]	2200
Cesium[a]	310–630
Neptunium[b]	unknown
Strontium[a]	56–200
Plutonium[a]	1100
Uranium[a]	6–13

a. Wolfsberg 1980
b. Triay et al. 1994

Krupka and Serne (1995) reviewed and generally agreed with the selected sorption data (Table 9) presented by Bradbury and Sarott (1995). Bradbury and Sarott (1995) provide detailed discussions on waste- and disposed-material-induced processes that influence the extent of sorption of different radionuclides under oxidizing and reducing conditions. We have selected values, based on observed mineralogy (Fe_2O_3, $Fe(OH)_3$, Fe_3O_4), of the sorption data for oxidizing conditions that prevail in the organic-poor unsaturated zone within the Bandelier Tuff.

TABLE 9

AVERAGE SORPTION RATIO, K_D OR R_D, (ML/G) FOR CEMENT [$CA(OH)_2$], OXIDIZING CONDITIONS, PH 12.5, 25°C[a]

Element	Cement
Actinium	2,000
Aluminum	5,000[b]
Americium	5,000
Barium	50.0[b]
Cadmium	500[b]
Californium	5,000[b]
Carbon (CO_3^{2-})	70,000
Cesium	20.0
Chlorine	20.0
Cobalt	100
Curium	5,000
Europium	5,000[b]
Gadolinium	5,000[b]
Hafnium	5,000
Hydrogen (tritium)	0
Iodine	0
Krypton	0
Lead	500
Molybdenum	0.1
Neptunium	5,000
Niobium	500
Nickel	100
Palladium	100
Plutonium	5,000
Potassium	0
Protactinium	5,000
Radium	50.0

a. Bradbury and Sarott 1995

b. Sorption ratios estimated as follows: Si(IV) is chemically similar to Sn(IV); Cd(II) is chemically similar to Pb(II); Ba(II) is chemically similar to Ra(II); and Al (III), Sm (III), Eu(III), Gd(III), and Cf(III) are chemically similar to Am(III). Hafnium (IV) is chemically similar to zirconium (IV).

TABLE 9 (concluded)

Element	Cement
Samarium	5,000[b]
Selenium	0.1
Silicon	1,000[b]
Silver	1.0
Strontium	1.0
Technetium	1.0
Thorium	5,000
Tin	1,000
Uranium	2,000
Zirconium	5,000

b. Sorption ratios estimated as follows: Si(IV) is chemically similar to Sn(IV); Cd(II) is chemically similar to Pb(II); Ba(II) is chemically similar to Ra(II); and Al (III), Sm (III), Eu(III), Gd(III), and Cf(III) are chemically similar to Am(III). Hafnium (IV) is chemically similar to zirconium (IV).

Fracture flow within the Bandelier Tuff and other hydrogeologic units may be significant beneath the pits at MDA G. Burkholder (1976) presents the following equation expressing the distribution coefficient, K_A, on a per unit of surface area basis.

$$K_A = \frac{\text{mass of solute on the solid phase per unit area of solid phase}}{\text{concentration of solute in solution}} \quad . \qquad (5)$$

The dimensions for Equation (5) are $[L^3/M \times M/L^2]$ or [L], and the units of Equation (5) are cm. Surface-area measurements (BET-N^2 gas method) of the Bandelier Tuff range between 0.4981 and 5.3856 cm^2/g (n = 21) with a mean of 1.5599 m^2/g (1.5599 x 10^4 cm^2/g) (Stephens and Associates 1994a). Using the K_D values listed in Tables 7 and 8 and an average surface area of 1.5599 x 10^4 cm^2/g for the Bandelier Tuff, K_A values were calculated (Table 10). These K_A values are quite low, suggesting that very little adsorption within fractures is likely based on the small surface area of the Bandelier Tuff.

A retardation equation for fracture flow presented by Freeze and Cherry (1979) is shown as Equation (6).

$$\frac{v}{v_c} = 1 + \frac{2K_A}{b} \quad , \qquad (6)$$

where v is the average flow velocity,
v_c is the average flow velocity of a given contaminant,
K_A is the distribution coefficient per unit of surface area, and
b is the aperture width of the fracture.

The ratio v/v_c is equivalent to the retardation factor. Equation (6) assumes that fracture surfaces are planer; however, some of the fracture surfaces at TA-54 are irregular and contain coatings of calcite, solid organic matter, smectite, kaolinite, and ferric oxyhydroxide(s) (Davenport, 1993). These coatings probably have higher surface areas than the Bandelier Tuff; therefore, the amount of sorption may be greater in filled or lined fractures than in unlined fractures. Fracture widths (parameter b) measured at MDA G consist of median apertures ranging between 0.2 and 0.4 cm (Reneau and Vaniman 1994). The mean fracture aperture on the lower walls of Pit 39 is 0.53 ± 1.11 cm (n = 122), although some fracture openings reached 10 cm in width (Reneau and Vaniman 1994).

Using the K_A values listed in Table 10 and a mean fracture aperture of 0.53 cm, retardation factors were calculated for fractured volcanic rock (Table 11). These retardation factors are quite low, suggesting that elements of concern will migrate at the same rate as water within the fractures.

TABLE 10

RANGES OF SORPTION RATIOS PER SURFACE AREA OF FRACTURED ROCK, K_A[a] (CM) FOR VOLCANIC ROCK, YUCCA MOUNTAIN AND BANDELIER TUFFS[b]

Element	Devitrified Tuff
Americium[c]	0.0083
Carbon	0
Cesium[c]	0.0096–0.0558
Cobalt[d]	0.00003
Iodine[c]	0
Neptunium[e]	0–0.00019
Plutonium[c]	0.0071
Strontium[c]	0.0034–0.0122
Technetium[c]	0.00002
Uranium[c]	0.00010–0.00014

a. $K_A = \frac{\text{mass of solute on the solid phase per unit area of solid phase}}{\text{concentration of solute in solution}}$

b. Average surface area of Bandelier Tuff is 1.5599 x 10^4 cm^2/g (Stephens and Associates 1994a).

c. Wolfsberg 1980

d. Polzer et al. 1985

e. Triay et al. 1994

Sorption and desorption ratios of Cs, Sr, Am, Pu, U, Np, I, Tc, and C are determined from Yucca Mountain tuffs, whereas the sorption ratio for Co is determined from the Bandelier Tuff.

TABLE 11

RANGES OF RETARDATION FACTORS[a] FOR FRACTURED VOLCANIC ROCK, K_A (CM) FOR VOLCANIC ROCK, YUCCA MOUNTAIN AND BANDELIER TUFFS

Element	Devitrified Tuff
Americium[b]	1.0313
Carbon	1.0
Cesium[b]	1.0362–1.2106
Cobalt[c]	1.0001
Iodine[b]	1.0
Neptunium[d]	1–1.0007
Plutonium[b]	1.0268
Strontium[b]	1.0128–1.0460
Technetium[b]	1.0001
Uranium[b]	1.0004–1.0005

a. Sorption and desorption ratios of Cs, Sr, Am, Pu, U, Np, I, Tc, and C are determined from Yucca Mountain tuffs, whereas the sorption ratio for Co is determined from the Bandelier Tuff. The retardation factor is given by $v/v_c = 1 + 2K_A/b$ where v is the average flow velocity, v_c is the average flow velocity of a given contaminant, K_A is the distribution coefficient per unit surface area, and b is the aperture width of the fracture. The mean fracture aperture on the lower walls of Pit 39, MDA G, is 0.53 cm (Reneau and Vaniman 1994).

b. Wolfsberg 1980

c. Polzer et al. 1985

d. Triay et al. 1994

4.3.2 Element-Radionuclide Rock/Water Interactions

The following discussion focuses on rock/water interactions, such as pH, Eh, solution composition, and presence of competing and complexing ligands, that have the greatest impact on the sorption behavior of the elements of concern present in the pits.

Knowledge of the redox conditions in the subsurface beneath MDA G is important. The Eh of solution in a rock/water system can influence the solubility and sorption behavior of a radionuclide. The sorption experiments cited in this report were conducted under relatively oxidizing conditions, which are likely to dominate at MDA G. Under these conditions, sorptive capacities of the Bandelier Tuff are predicted to decrease for U, Pu, Np, and Tc, which are stable in higher oxidation states, based on experimental results reported by Wolfsberg (1980) and Triay et al. (1994). Solubilities of these elements in solid phase are much lower under relatively reducing conditions than they are under relatively oxidizing conditions (Brookins 1988). Oxidizing Eh values should be used in any proposed experimental work and in model simulations.

The effect of ligand competition on the sorptive behavior of some elements of concern may be of secondary importance at MDA G. Radionuclides that adsorb/desorb by ion exchange, including ^{137}Cs and ^{90}Sr, may have higher affinities for ion-exchange sites available in the Bandelier Tuff than the major cations (Na^+, Ca^{2+}, Mg^{2+}, and K^+) present in Pajarito Plateau groundwaters. The sorptive capacities of the Bandelier Tuff for ^{137}Cs and ^{85}Sr, however, could be quite low (^{137}Cs at 0.661 ml/g and ^{85}Sr at 0.224 ml/g) (Polzer et al. 1985).

Changes in pH can have a major effect on the adsorption behavior of U, Pu, Am, and Np, where adsorption is controlled by surface complexation processes. When a net negative surface charge dominates on the adsorbent before the sorption reaction, sorption of cationic complexes is maximized above the pH of point of zero charge (pH_{pzc}). Conversely, when a net positive surface charge dominates on the adsorbent before the sorption reaction, sorption of anionic complexes is maximized below the pH_{pzc}. Anionic complexes of U, Am, Np, Pu, and Tc tend to adsorb less than cationic complexes at pH values greater than the pH_{pzc} for specific adsorbents. Cationic species of the elements of concern adsorb onto smectite and ferric oxyhydroxide to a greater extent than anionic species at pH 7 and higher (Triay et al. 1994, Brookins 1984, GCX 1994). Cationic adsorbates are expected to adsorb onto solid surfaces to a greater extent than anionic adsorbates.

For many of the elements of concern, the value of K_D is in part controlled by competition between the sorbent/surface site and complexing ligands (Cl^-, F^-, CO_3^{2-}, HCO_3^-, PO_4^{3-}, SO_4^{2-}) present in solution and dissociated organic anions such as humic and fulvic acids. By increasing the concentration of a complexing ligand in solution, the value of K_D is typically decreased. Aqueous speciation of elements of concern is provided in Table 12, with the listed values based on spectroscopy and/or thermodynamic calculations. Analytical results of groundwater samples collected on the Pajarito Plateau show that HCO_3^- is the anion found in highest concentration, typically exceeding millimolar concentrations. This ligand is important for radionuclide complexing of Np, Pu, and U in natural solutions (Clark et al. 1995). Increases in ligand concentration, however, may enhance precipitation of the element, e.g., the mineral UO_2CO_3, results in a decrease in solution concentration. Therefore, concentrations of ligands, including HCO_3^-, should be determined in porewaters for geochemical modeling simulations and experimental studies of MDA G.

4.3.3 Element-Radionuclide Solubility Limits

This section discusses solubility limits for the elements of concern in pits at TA-54. Solubilities of the elements of concern will be controlled by the degradation of wastes, e.g., corrosion of metal, breakdown of cardboard, and dissolution of soluble constituents within the concrete. Table 13 provides a summary of solubilities of solid phases for elements C, Sr, and U. Solid phases of U probably occur in waste as U metal and as U(IV) and U(VI). The values for C, Sr, and U are based on Yucca Mountain Project experiments and on thermodynamic calculations using the geochemical code MINTEQA2 (Allison et al. 1991). Solubility of $CoCO_3$ was estimated from thermodynamic data tabulated in Woods and Garrels (1987). These calculations were performed assuming an open system with CO_2 gas ($PCO_2 = 10^{-2.11}$ atm) (Kunkler 1969a, 1969b) to simulate

vadose-zone conditions within the Bandelier Tuff. Measured solubilities were available for Am, Pu, and Np (Triay et al. 1994, Nitsche et al. 1993). Molal solubilities for solid phases (Table 13) containing C, Co, Sr, and U were calculated using analytical results from native (background) groundwater discharging from the Bandelier Tuff in Water Canyon. Analytical results of groundwater collected at the Water Canyon Gallery are provided in Table 6. This native groundwater probably is representative of recharge (noncontaminated) pore water within the pits. Concentrations of Cl, NO_3, and PO_4 are less than 1 mg/kg, suggesting that anthropogenic species are not present. The TDS content is 106 mg/kg, which is relatively low compared to other groundwater samples collected on the Pajarito Plateau (Blake et al. 1995, Adams 1994).

TABLE 12

RESULTS OF SPECIATION INVESTIGATIONS (MEASURED AND CALCULATED) FOR SELECTED ELEMENTS AT PH 7 WITH PCO_2 EQUAL TO $10^{-2.11}$ ATM UNDER OXIDIZING CONDITIONS AT 25°C

Element	Aqueous Species
Americium[a]	$AmCO_3^+$, $Am(CO_3)_2^-$
Carbon[b]	HCO_3^- (35%), $CaHCO_3^+$ (58%)
Cesium	Cs^+
Cobalt[c]	Co^{2+}
Iodine	I^-
Neptunium[a]	NpO_2^+ (46%), $NpO_2CO_3^-$ (54%)
Plutonium[a]	III^++ polymer, 5%; IV^+, 6%; V^+, 73% ; VI^+, 18%
Strontium[b]	Sr^{2+}
Technetium	TcO_4^-
Tritium	^3HHO
Uranium[b]	$UO_2(CO_3)_2^{2-}$ (81%), $(UO_2)_3(OH)_5^+$ (1%), $UO_2CO_3^0$(16%), $UO_2(CO_3)_3^{4-}$ (2%)

a. Speciation for Am, Np, and Pu were measured by Nitsche et al. (1993), Triay et al. (1994), and GCX (1994).

b. Speciation calculations for C, Sr, and U were performed using the geochemical computer program MINTEQA2 (Allison et al. 1991). Partial pressure of CO_2 gas set equal to $10^{-2.11}$ atmosphere for the computer simulations.

c. Speciation calculations for Co were performed using data from Brookins (1988). Input data for simulations are described in the text using chemical analyses from Water Canyon Gallery discharging from the Bandelier Tuff, Los Alamos, New Mexico.

Table 14 provides a summary of solubilities of solid phases at pH 12 using data provided by Ewart et al. (1989). Geochemical modeling was also performed on specific elements (Se, U, Cd, Al, and Si). The geochemical code MIMTEQA2 was used and equilibium with $Ca(OH)_2$ was assumed (Allison et al. 1991). Solubilities for nonredox sensitive elements are assumed to be constant, provided that the solid-phase controlling element solubility

reported by Ewart et al. (1989), which was measured under reducing conditions, applies for oxidizing conditions at TA-54.

TABLE 13

PRELIMINARY MEASURED AND CALCULATED SOLUBILITIES FOR SELECTED ELEMENTS IN VOLCANIC TUFF AT PH 7, 25°C[a]

Element	Solubility (mol/kg)	Element	Solubility (mol/kg)
Hydrogen	very large	Californium[d]	1.2×10^{-9}
Cesium	large	Europium[d]	1.2×10^{-9}
Strontium[b]	0.0014	Barium[b]	4.5×10^{-5}
Silicon[b]	2.8×10^{-4}	Aluminum[b]	3.5×10^{-11}
Americium[a]	1.2×10^{-9}	Curium[d]	1.2×10^{-9}
Plutonium[a]	2.3×10^{-7}	Protactinium[e]	1.3×10^{-4}
Thorium	1.9×10^{-10}	Radium[c]	5.5×10^{-11}
Samarium[a]	1.2×10^{-9}	Tin[c]	4.3×10^{-37}
Gadolinium[a]	1.2×10^{-9}	Molybdenum	large
Iodine	very large	Silver[b]	5.6×10^{-10}
Uranium[b]	1.1×10^{-4}	Palladium	1.0×10^{-5}
Carbon[a]	0.00034	Chlorine	very large
Technetium	large	Lead[b]	1.6×10^{-6}
Cobalt[c]	1.7×10^{-7}	Niobium[c]	2.0×10^{-54}
Zirconium[c]	1.0×10^{-15}	Selenium[b]	0.0079
Nickel[b]	1.0×10^{-5}	Neptunium[a]	1.3×10^{-4}
Cadmium[b]	5.0×10^{-8}	Actinium[d]	1.2×10^{-9}
Hafnium[c]	1.0×10^{-15}	—	—

a. Solubilities for Am, Np, and Pu were measured by Nitsche et al. (1993), Triay et al. (1994), and GCX (1994).

b. Solubilities for different elements were calculated using the geochemical computer program MINTEQA2 (Allison et al. 1991).

c. Solubilities for elements were calculated from thermodynamic data and redox information presented in Brookins (1988).

d. Solubilities were estimated based on chemical similarities with Am(III).

e. Solubilities were estimated based on chemical similarities with Np(V). Input data for simulations consist of chemical analyses from Water Canyon Gallery discharging from the Bandelier Tuff, Los Alamos, New Mexico.

4.4. Uncertainties and Further Investigations

Geochemical and hydrological processes influencing solute-transport processes in the Bandelier Tuff are extremely complex. Literature values from the Yucca Mountain Project (Triay et al. 1994) for geochemical calculations used in this report are reasonable

estimates for approximating solute transport in volcanic rock. There are uncertainties, however, associated with the application of these data to MDA G, which include

TABLE 14

PRELIMINARY MEASURED AND CALCULATED SOLUBILITIES[a] FOR SELECTED ELEMENTS AT PH 12, 25°C

Element	Solubility (mol/kg)	Element	Solubility (mol/kg)
Hydrogen	very large	Californium[b]	$3x10^{-11}$
Cesium[b]	large	Europium[b]	$1x10^{-10}$
Strontium[b]	$4x10^{-4}$	Barium[b]	$4x10^{-4}$
Silicon[c]	0.118	Aluminum[c]	0.250
Americium[b]	$3x10^{-11}$	Curium[b]	$3x10^{-11}$
Plutonium[b]	10^{-8} to 10^{-10}	Protactinium[b]	$1x10^{-10}$
Thorium[b]	$1x10^{-9}$	Radium[b]	$1x10^{-7}$
Samarium[b]	$1x10^{-10}$	Tin[b]	0.005
Gadolinium[b]	$1x10^{-10}$	Molybdenum[b]	large
Iodine[b]	very large	Silver[b]	$1x10^{-4}$
Uranium[b]	$4x10^{-7}$	Palladium[b]	$1x10^{-7}$
Carbon[b]	$3x10^{-5}$	Chlorine[b]	very large
Technetium[b]	large	Lead[b]	$4x10^{-4}$
Cobalt[d]	$8x10^{-17}$	Niobium[b]	$1x10^{-7}$
Zirconium[b]	$1x10^{-8}$	Selenium[c]	$3x10^{-5}$
Nickel[b]	$1x10^{-7}$	Neptunium[b]	10^{-8} to 10^{-7}
Cadmium[c]	0.069	Actinium	$1x10^{-10}$
Hafnium[e]	$1x10^{-8}$		

a. Input data for simulations consist of chemical analyses from Water Canyon Gallery discharging from the Bandelier Tuff, Los Alamos, New Mexico.

b. Solubility data are from Ewart et al. (1989).

c. Solubilities for Se, U, Cd, Al, and Si were calculated using the geochemical computer program MINTEQA2 (Allison et al. 1991). U(VI) is assumed to be in equilibrium with $CaUO_4$ (personal communication with R. J. Serne on April 26, 1995). Se(IV) is assumed to be in equilibrium with $CaSeO_3 \cdot H_2O$, based on moderate oxidizing conditions and a pore water enriched with Ca^{2+} from the dissolution of portlandite cement. Cd(II) is assumed to be in equilibrium with amorphous $Cd(OH)_2$ under high pH conditions. Al(III) is assumed to be in equilibrium with amorphous $Al(OH)_3$ under high pH conditions. Si(IV) is assumed to be in equilibrium with SiO_2 glass under high pH conditions.

d. Co(II, III) is assumed to be in equilibrium with Co_3O_4, (Brookins 1988) under high pH and oxidizing conditions (Eh = 250 mV).

e. Hafnium (IV) is chemically similar to zirconium (IV).

Solubilities for nonredox sensitive elements are assumed to be constant, provided that the solid phase controlling element solubility reported by Ewart et al. (1989) measured under reducing conditions apply for oxidizing conditions. Log PCO_2 gas set at -5 for model simulations.

application to field conditions at TA-54, laboratory-based sorption investigations as opposed to site-specific field calibrated investigations, mineralogy of waste/waste form(s), chemical characteristics of pore water, and sorption processes for matrix and fracture flow.

Site-specific data are required as input to FEHM (Zyvolski et al. 1988) to obtain the most relevant and meaningful results for the performance assessment. Geochemical data needs for model input using FEHM (Zyvoloski et al. 1988) include sorption isotherm models, consisting of linear (K_D), Freundlich, modified Freundlich, and Langmuir; Henry's Law constants for liquid and vapor species; chemical rate laws using the Arrhenius equation; and solubility data for solid phases. The release of elements-radionuclides from the pits will be controlled by hydraulic flux, pore-water chemistry, mineral solubility, and sorption behavior. Data and information needs to verify and quantify geochemical reactions occurring at MDA G include source-term characterization (types, forms, and amounts of contaminants); source-term geochemistry (mineralogy, speciation, solubility, sorption, pore-water chemistry, and reaction rates); and hydrogeological/geochemical characterization of Bandelier Tuff and other geologic media at the site (mineralogy, fracture distribution, fracture mineralogy, sorption capacity of fracture material, hydraulic conductivity, porosity, and moisture content).

ACKNOWLEDGMENTS

The authors appreciate the reviews of earlier drafts by and helpful discussions with David Rogers, Everett Springer, and Diana Hollis. The work was supported by Contract W-7405-ENG-36.

REFERENCES

Abeele, W. V., "Determination of Relative Hydraulic Conductivity from Moisture Retention Data Obtained in the Bandelier Tuff," Los Alamos Scientific Laboratory report LA-7625-MS (January 1979a).

Abeele, W. V., "Determination of Hydraulic Conductivity in Crushed Bandelier Tuff," Los Alamos Scientific Laboratory report LA-8147-MS (November 1979b).

Abeele, W. V., "Hydraulic Testing of Crushed Bandelier Tuff," Los Alamos National Laboratory report LA-10037-MS (March 1984).

Abeele, W. V., H. R. Fuentes, and J. Hosch, "Characterization of Soil Moisture Characteristic Curves in the 30 to 1000 kPa Tension Range for Bandelier Tuff in Waste Disposal Areas G and L, Technical Area 54, Los Alamos National Laboratory," Los Alamos National Laboratory report LA-UR-86-4360 (September 1986).

Abeele, W. V., M. L. Wheeler, and B. W. Burton, "Geohydrology of Bandelier Tuff," Los Alamos National Laboratory report LA-8962-MS (October 1981).

Abrahams, J. H., Jr., "Physical Properties of and Movement of Water in the Bandelier Tuff, Los Alamos and Santa Fe Counties, New Mexico," US Geological Survey Administrative Release, Albuquerque, NM (January 1963).

Allison, J. D., D. S. Brown, and K. J. Novo-Gradac, "MINTEQA2/PRODEFA2, A Geochemical Assessment Model for Environmental Systems: Version 3.0 User's Manual," EPA/600/3-91/021 (US Environmental Protection Agency, Athens, Georgia, 1991).

Baltz, E. H., J. H. Abrahams, Jr., and W. D. Purtymun, "Preliminary Report on the Geology and Hydrology of Mortandad Canyon near Los Alamos, New Mexico, with Reference to Disposal of Liquid Low-Level Radioactive Waste," USGS Open-File Report, Albuquerque, New Mexico (March 1963).

Bear, J., *Dynamics of Fluids in Porous Media* (American Elsevier Publishing, New York, 1972).

Berner, U. R., "Evolution of Pore Water Chemistry During Degradation of Cement in A Radioactive Waste Repository," *Waste Management* **12**, 201–219 (1992).

Blake, W. D., F. Goff, A. I. Adams, and D. Counce, "Environmental Geochemistry for Surface and Subsurface Waters in the Pajarito Plateau and Outlying Areas, New Mexico," Los Alamos National Laboratory report LA-12912-MS (1995).

Bradbury, M. H. and F. A. Sarott, "Sorption Databases for the Cementatious Near-Field of a L/ILW Repository for Performance Assessment," (Paul Scherrer Institut, 1995) PSI Bericht Nr. 95-06.

Brookins, D. G., *Geochemical Aspects of Radioactive Waste Disposal* (Springer-Verlag, New York, 1984).

Brookins, D. G., *Eh-pH Diagrams for Geochemistry* (Springer-Verlag, New York, 1988).

Broxton, D. E. and P. G. Eller (eds.), "Earth Science Investigations for Environmental Restoration—Los Alamos National Laboratory Technical Area 21," Los Alamos National Laboratory report LA-12934-MS (June 1995).

Broxton D. and S. Reneau, "Stratigraphic Nomenclature of the Bandelier Tuff for the Environmental Restoration Project at Los Alamos National Laboratory," Los Alamos National Laboratory report LA-13010-MS (1995).

Broxton, D. E., C. LaDelfe, S. J. Chipera, and E. C. Kluk, "Stratigraphy, Mineralogy and Chemistry of Bedrock Tuffs at Mesita del Buey, Los Alamos National Laboratory, New Mexico," Los Alamos National Laboratory report (in progress).

Broxton, D. E., G. Heiken, S. J. Chipera, and F. M. Byers Jr., "Stratigraphy, Petrography, and Mineralogy of Tuffs at Technical Area 21, Los Alamos National Laboratory, New Mexico": in "Phase Report 1A, TA-21 Operable Unit RCRA Facility Investigation," Los Alamos National Laboratory report LA-UR-93-2028 (1995) pp. A1-A18.

Burkholder, H. C., "Methods and Data for Predicting Nuclide Migration in Geologic Media," in International Symposium Management of Wastes from the LWR Fuel Cycle, Denver, Colorado (1976).

Caporuscio, F. A., "Description of Rock Units in Drill Core at TA-54 Los Alamos National Laboratory," letter report (June 1994).

Clark, D. L., D. E. Hobart, and M. P. Neu, "Actinide Carbonate Complexes and Their Role in Actinide Environmental Chemistry," *Chem. Rev.* (1995), in press.

Conca, J. L. and J. Wright, "Direct Determination s of Unsaturated Flow and Transport," in Proceedings of the Twelfth Annual American Geophysical Union Hydrology Days Meeting (Hydrology Days Publications, Fort Collins, Colorado, March 1992).

Cooper, J. B., W. D. Purtymun, and E. C. John, "Records of Water-Supply Wells Guaje Canyon 6, Pajarito Mesa 1, and Pajarito Mesa 2, Los Alamos, New Mexico, Basic Data Report" USGS Administrative Release, Albuquerque, New Mexico (July 1965).

Crowe, B., G. Linn, G. Heiken, and M. Bevier, "Stratigraphy of the Bandelier Tuff in the Pajarito Plateau, Applications to Waste Management," Los Alamos National Laboratory report LA-7225-MS (1978).

Davenport, D. W., "Micromorphology, Mineralogy, and Genesis of Soils and Fracture Fills on the Pajarito Plateau, New Mexico," Ph. D. Dissertation, Texas Tech University (1993).

Devaurs, M., "Core Analyses and Observation Well Data from Mesita del Buey Waste Disposal Areas and in Adjacent Canyons," Los Alamos National Laboratory report LA-UR-85-4003 (1985).

Devaurs, M. and W. D. Purtymun, "Hydrologic Characteristics of the Alluvial Aquifers in Mortandad, Cañada del Buey, and Pajarito Canyons," Los Alamos National Laboratory report LA-UR-85-4002 (1985).

Ewart, F. T, S. Y. Pugh, S. J. Wisbey, and D. R. Woodwark, "Chemical and Microbial Effects in the Near Field: Current Status 1989," Harwell Laboratory, UKAEA, report G/111, (1989).

Freeze, R. A. and J. A. Cherry, *Groundwater*, (Prentice-Hall, Inc., Englewood Cliffs, New Jersey, 1979).

Fuentes, H. R., W. L. Polzer, J. Gruber, B. Lauctes, and E. H. Essington, "Preliminary Report on Sorption Modeling," Los Alamos National Laboratory report LA-10952-MS, (1987).

Gardner, J. N., T. Kolbe, and S. Chang, "Geology, Drilling, and Some Hydrologic Aspects of Seismic Hazards Program Core Holes, Los Alamos National Laboratory, New Mexico," Los Alamos National Laboratory report LA-12460-MS (January 1993).

GCX, "Groundwater Compositional Parameters Most Critical to the Sorption Behavior of Radionuclides-Of-Concern to the Yucca Mountain Project Milestone 4032 Letter Report," prepared for Los Alamos National Laboratory and Yucca Mountain Site Characterization Office (1994).

Goff, F., "Geologic Map of Technical Area 21," in "Earth Science Investigation for Environmental Restoration, Los Alamos National Laboratory Technical Area 21," D. E. Broxton and P. G. Eller, eds., Los Alamos National Laboratory report LA-12934-MS (1995).

Griggs, R. L., "Geology and Groundwater Resources of the Los Alamos Area, New Mexico, with a section of Quality of Water (John D. Hem)," US Geological Survey Water-Supply Paper 1753 (1964).

Heiken, G., F. Goff, J. N. Gardner, W. S. Baldridge, J. B. Hulen, D. L. Nielson, and D. Vaniman, "The Valles/Toledo Caldera Complex, Jemez Volcanic Field, New Mexico," in *Annual Review of Earth Planetary Science*, Vol. 18, pp. 27-53 (1990).

Kearl, P. M., J. J. Dexter, and M. Kautsky, "Vadose Zone Characterization of Technical Area 54, Waste Disposal Areas G and L, Los Alamos National Laboratory, New Mexico. Report 3: Preliminary Assessment of the Hydrogeologic System," Bendix Field Engineering Corp., Grand Junction Operations, Colorado, report GJ-44 (March 1986a).

Kearl, P. M., J. J. Dexter, and M. Kautsky, "Vadose Zone Characterization of Technical Area 54, Waste Disposal Areas G and L, Los Alamos National Laboratory, New Mexico. Report 4: Preliminary Assessment of the Hydrologic System Through Fiscal Year 1986," UNC Technical Services, Inc., Grand Junction, Colorado, report GJ-54 (December 1986b).

Klute, A., "Water Retention: Laboratory Methods," in *Methods of Soil Analysis, Part 1. Physical and Mineralogical Methods, Agronomy Monograph No. 9* (American Society of Agronomy-Soil Science Society of America, 1986), pp. 635-662.

Krupka, K. M. and R. J. Serne, "Performance Assessment of Low-Level Radioactive Waste Disposal Facilities: Effects on Radionuclide Concentrations by Cement/Ground-Water Interactions," Earth and Environmental Sciences Center, Pacific Northwest Laboratory, Richland, WA, Draft Document NUREG/CR, (1995).

Kunkler, J. L., "The Sources of CO_2 in the Zone of Aeration of the Bandelier Tuff Near Los Alamos, New Mexico," US Geological Survey Professional Paper 650-B (1969a), B185-B188.

Kunkler, J. L., "Measurement of Atmospheric Pressure and Subsurface-Gas Pressure in the Unsaturated Zone of the Bandelier Tuff, Los Alamos, New Mexico," US Geological Survey Professional Paper 650-D, (1969b), D283-D287.

LANL, "RFI Report for PRS 54-006," Los Alamos National Laboratory report (in progress).

LANL, "RFI Work Plan for Operable Unit 1098, Environmental Restoration Program," Los Alamos National Laboratory report LA-UR-92-3825 (May 1993).

Longmire, P., C. Duffy, and S. Reneau, "Preliminary Background Elemental Concentrations In Bandelier Tuff and Selected Soil Series, 1993," unpublished report, Los Alamos National Laboratory (1993).

Longmire, P., S. Reneau, P. Watt, L. McFadden, J. Gardner, C. Duffy, and R. Ryti, "Natural Background Geochemistry, Geomorphology, and Pedogenesis of Selected Soil Profiles and Bandelier Tuff, Los Alamos, New Mexico," Los Alamos National Laboratory report LA-12913-MS (1995) in press.

Los Alamos Technical Associates, "Assessment of Potential Shallow Groundwater Transport of Radionuclides at Critical Experiment Facility, TA-18, Los Alamos National Laboratory," (January 1991).

Martens, S. and F. Barnes, "Report on Activities for the Pilot Program for Root Distribution Studies FY 93," Los Alamos National Laboratory memorandum ESH15-93-533 to D. A. Neeper (September 1993).

Meijer, A., "Far-Field Transport of Carbon Dioxide: Retardation Mechanisms and Possible Validation Experiments," *in* Proceedings of the Topical Meeting Site Characterization and Model Validation Focus '93, September 26-29, 1993, Las Vegas, Nevada (American Nuclear Society, La Grange Park, Illinois) (1993), 110-112.

Mualem, Y., "A New Model for Predicting the Hydraulic Conductivity of Unsaturated Porous Media," *Water Resources Research* **12**, 512–522 (1976).

Nitsche, H., R. C. Gatti, E. M. Standifer, S. C. Lee, A. Muller, T. Prussin, R. S. Deinhammer, H. Maurer, K. Becraft, S. Leung, and S. A. Carpenter, "Measured Solubilities and Speciations of Neptunium, Plutonium, and Americium in a Typical Groundwater (J-13) from the Yucca Mountain Region, Milestone Report 3010-WBS 1.2.3.4.1.3.1," Los Alamos national Laboratory report LA-12562-MS (1993).

Polzer, W. L., H. R. Fuentes, E. H. Essington, and F. R. Roensch, "Equilibrium Sorption of Cobalt, Cesium, and Strontium on Bandelier Tuff: Experiments and Analysis," Waste Management 1985 (1985), 175-181.

Polzer, W. L., M. G. Rao, H. R. Fuentes, and R. J. Beckman, "Thermodynamically Derived Relationships Between the Modified Langmuir Isotherm and Experimental Parameters," *Environmental Science and Technology*, **26**, 1780–1786 (1992).

Purtymun, W. D., "Hydrologic Characteristics of the Main Aquifer in the Los Alamos Area: Development of Ground Water Supplies," Los Alamos National Laboratory report LA-9957-MS (January 1984).

Purtymun, W. D., "Geologic and Hydrologic Records of Observation Wells, Test Holes, Test Well, Supply Wells, Springs, and Surface Water Stations in the Los Alamos Area," Los Alamos National Laboratory report LA-12883-MS (January 1995).

Purtymun, W. D., and J. B. Cooper, "Development of Ground-Water Supplies on the Pajarito Plateau, Los Alamos County, New Mexico," in Geological Survey Research 1969, US Geological Survey Professional Paper No. 650-B, pp. B149-B153 (1969).

Purtymun, W. D. and W. R. Kennedy, "Geology and Hydrology of Mesita del Buey," Los Alamos Scientific Laboratory report LA-4460 (May 1971).

Purtymun, W. D., E. A. Enyart, and S. G. McLin, "Hydrologic Characteristics of the Bandelier Tuff as Determined Through an Injection Well System," Los Alamos National Laboratory report LA-11511-MS (August 1989).

Purtymun, W. D., M. L. Wheeler, and M. A. Rogers, "Geologic Description of Cores from Holes P-3 MH-1 Through P-3 MH-5, Area G, Technical Area 54," Los Alamos National Laboratory report LA-7308-MS (May 1978).

Reneau, S. L. and D. T. Vaniman, "Fracture Characteristics in a Disposal Pit on Mesita del Buey, Los Alamos National Laboratory," Los Alamos National Laboratory unpublished report (March 21, 1994).

Reneau, S. L., T. Kolbe, D. Simpson, J. S. Carney, J. N. Gardner, S. S. Olig, and D. T. Vaniman, "Surficial Materials and Structure at Pajarito Mesa," in "Geological Site Characterization for the Proposed Mixed Waste Disposal Facility, Los Alamos National Laboratory," S. L. Reneau and R. Raymond, eds., Los Alamos National Laboratory report LA-13089-MS (1995).

Rogers, D. B., "Unsaturated Hydraulic Characteristics of the Bandelier Tuff at TA-54," Los Alamos National Laboratory memorandum ESH-18/WQ&H-94-565 (November 17, 1994).

Rogers, D. B. and B. M. Gallaher, "Moisture and Matric Suction Profiles for 1994 MDA G Wells," Los Alamos National Laboratory memorandum ESH-18/WQ&H-94-632 to J. Turin (December 19, 1994a).

Rogers, D. B. and B. M. Gallaher, "Unsaturated Hydraulic Characteristics of the Bandelier Tuff," Los Alamos National Laboratory memorandum ESH-18/WQ&H-94-525 (October 31, 1994b).

Rogers, D. B. and B. M. Gallaher, "The Unsaturated Hydraulic Characteristics of the Bandelier Tuff," Los Alamos National Laboratory report LA-12968-MS (September 1995).

Rogers, M. A., "History and Environmental Setting of LASL Near-Surface Land Disposal Facilities for Radioactive Wastes (Areas A, B, C, D, E, F, G, and T)", Los Alamos Scientific Laboratory report LA-6848-MS, Vol. 1 (June 1977).

Rosenberg, N. D. and H. J. Turin, "Summary of Area G Geology, Hydrology, and Seismicity for Radiological Performance Assessment," Los Alamos National Laboratory report LA-UR-93-3081 (August 1993).

Rundberg, R. S., "Assessment Report on the Kinetics of Radionuclide Adsorption on Yucca Mountain Tuff," Los Alamos National Laboratory report LA-11026-MS (1987).

Science and Engineering Associates, "Data Report: Open Borehole Anemometry and In Situ Gas Permeability Measurements in Boreholes 54-1001 Through 54-1006, Los Alamos Technical Area 54," performed for Los Alamos National Laboratory Contract 9-XZ3-2348K-1 (December 1994; revised March 1995).

Smith, R. L. and R. A. Bailey, "The Bandelier Tuff, a Study of Ash-Flow Eruption Cycles from Zoned Magma Chambers," *Bulletin Volcanique* **29**, 83–104 (1966).

Smith, R. L., R. A. Bailey, and C. S. Ross. "Geologic Map of Jemez Mountains, New Mexico: US Geological Survey Miscellaneous Investigations Series, Map I-571, Washington, D.C (1970).

Stephens, D. B. and Associates, "Laboratory Analysis of Soil Hydraulic Properties of Boreholes 54-1001, -1002, -1003, and -1006," subcontract XT1-X1785-1 report prepared for Los Alamos National Laboratory (1994a).

Stephens, D. B. and Associates, "Laboratory Analysis of Soil Hydraulic Properties of SHB Soil Samples," prepared for Los Alamos National Laboratory (August 1994b).

Stephens, D. B. and Associates, "Laboratory Analysis of Soil Hydraulic Properties of PC4 Pressure Plate and SPOC Samples," prepared for Los Alamos National Laboratory (1992a).

Stephens, D. B. and Associates, "Laboratory Analysis of Hydraulic Properties of Volcanic Tuff Samples," report to E. P. Springer for Subcontract 9-XT1-X1785-1, Los Alamos National Laboratory (1991).

Stephens, D. B. and Associates, "Laboratory Analysis of Soil Hydraulic Properties of CDBM 2 and CDBM 3 Samples," report to Alan Stoker for Subcontract 9-XT1-X27EE-1, Los Alamos National Laboratory (1992b).

Thibault, D. H., M. I. Sheppard, and P. A. Smith, "A Critical Compilation and Review of Default Soil Solid/Liquid Partition Coefficients, K_d, for Environmental Assessments," Whiteshell Nuclear Research Establishment report AECL-10125, Pinawa, Manitoba, Cañada ROE 1L0 (1990).

Thomas, K. W., "Summary of Sorption Measurements Performed with Yucca Mountain, Nevada, Tuff Samples and Water from Well J-13," Los Alamos National Laboratory report LA-10960-MS (1987).

Triay, I. R., C. R. Cotter, S. M. Kraus, M. H. Huddleston, S. J. Chipera, and D. L. Bish, "Report on Radionuclide Sorption in Yucca Mountain Tuffs with J-13 Well Water: Neptunium, Uranium, and Plutonium Milestone #3338," Los Alamos National Laboratory draft (1994).

van Genuchten, M. T., "A Closed-Form Equation for Predicting the Hydraulic Conductivity of Unsaturated Soils," *Soil Science Society of America Journal* **44**, 892–898 (1980).

van Genuchten, M. T., F. J. Leij, and S. R. Yates, "The RETC Code for Quantifying the Hydraulic Functions of Unsaturated Soils," US EPA report EPA/600/2-91/065 (December 1991).

Vaniman, D. and K. Wohletz, "Results of Geological Mapping/Fracture Studies: TA-55 Area," Los Alamos National Laboratory memorandum EES1-SH90-17. (November 14, 1990)

Vaniman, D. and K. Wohletz, "Revisions to Report EES1-SH90-17," Los Alamos National Laboratory memorandum EES1-SH91-12 (1991).

Weir, J. E., Jr., and W. D. Purtymun, "Geology and Hydrology of Technical Area 49, Frijoles Mesa, Los Alamos County, New Mexico," US Geological Survey Administrative Release, Albuquerque, New Mexico (1962).

Wolfsberg, K., "Sorptive Properties of Tuff and Nuclide Transport and Retardation," in "Evaluation of Tuff as a Medium for Nuclear Waste Repository: Interim Status Report on the Properties of Tuff," J. K. Johnstone and K. Wolfsberg, Eds., Sandia National Laboratory report SAND80-1464 (1980), pp. 39-48.

Woods, T. L. and R. M. Garrels, *Thermodynamic Values at Low Temperature for Natural Inorganic Materials: An Uncritical Summary* (Oxford University Press, New York, 1987).

Zyvoloski, G. A., Z. V. Dash, and S. Kelkar, "FEHM: Finite Element Heat and Mass Transfer Code," Los Alamos National Laboratory report LA-11224-MS (1988).